JGR Earth Surface

RESEARCH ARTICLE
10.1029/2025JF008590

Subglacial Topography of Coats Land Records Post-Gondwanan Landscape Evolution and Early Ice-Sheet Behavior in East Antarctica

Guy J. G. Paxman[1], Tom A. Jordan[2], Michael J. Bentley[1], David Small[1], Stewart S. R. Jamieson[1], and Daniel Steinhage[3]

[1]Department of Geography, Durham University, Durham, UK, [2]British Antarctic Survey, Cambridge, UK, [3]Alfred-Wegener-Institut, Helmholtz-Zentrum für Polar- und Meeresforschung, Bremerhaven, Germany

Key Points:

- Analysis of radio-echo sounding data and satellite imagery reveals a subglacial landscape that did not form beneath the modern ice sheet
- Geophysical modeling indicates that asymmetric troughs and highlands formed via extensional deformation associated with Gondwana breakup
- The landscape was then modified by fluvial planation and south-to-north ice flow before the modern ice configuration became established

Supporting Information:

Supporting Information may be found in the online version of this article.

Correspondence to:

G. J. G. Paxman,
guy.j.paxman@durham.ac.uk

Citation:

Paxman, G. J. G., Jordan, T. A., Bentley, M. J., Small, D., Jamieson, S. S. R., & Steinhage, D. (2026). Subglacial topography of Coats Land records post-Gondwanan landscape evolution and early ice-sheet behavior in East Antarctica. *Journal of Geophysical Research: Earth Surface*, *131*, e2025JF008590. https://doi.org/10.1029/2025JF008590

Received 21 MAY 2025
Accepted 27 JAN 2026

Author Contributions:

Conceptualization: Guy J. G. Paxman, Tom A. Jordan
Formal analysis: Guy J. G. Paxman
Investigation: Guy J. G. Paxman, Tom A. Jordan, Michael J. Bentley, David Small, Stewart S. R. Jamieson
Methodology: Guy J. G. Paxman, Tom A. Jordan
Resources: Daniel Steinhage
Writing – original draft: Guy J. G. Paxman
Writing – review & editing: Tom A. Jordan, Michael J. Bentley, David Small, Stewart S. R. Jamieson, Daniel Steinhage

Abstract The East Antarctic Ice Sheet (EAIS) formed circa 34 million years ago and now contains an ice volume equivalent to ~52 m of global sea-level rise. Although the EAIS is approximately in balance today, there is substantial uncertainty regarding the sensitivity of sectors underlain by low-lying bed topography to future climate and ocean warming. This is especially pertinent for Coats Land (eastern Weddell Sea), where geological records of past ice-sheet changes are sparse. Here, we use airborne radio-echo sounding and magnetic data, satellite imagery, and isostatic modeling to map the subglacial geomorphology of Coats Land for the first time and constrain the regional geological and ice-sheet history. Our mapping reveals topographic features such as tilted highlands and deep, asymmetric depressions, which likely formed via regional extension associated with Gondwana breakup, concomitant with early Jurassic magmatism. We also document low-relief, seaward-dipping surfaces that we infer to be remnants of coastal plains formed by fluvial erosion after continental breakup. Subglacial troughs that were incised into (i.e., post-date) these pre-glacial erosion surfaces were selectively eroded by ice flowing south-to-north. The ice within these troughs is stagnant today, indicating that they did not form beneath the modern (east-to-west-flowing) EAIS. Based on local geomorphological and geochronological evidence, we infer that these troughs were most likely incised during an interval of the Oligocene–Miocene (ca. 34–14 Ma) when the regional ice configuration and bed topography were significantly different from today. Subsequent EAIS reconfiguration switched off these early outlets and facilitated widespread landscape preservation beneath regionally non-erosive ice.

Plain Language Summary Approximately 80% of Earth's ice can be found in the East Antarctic Ice Sheet. Although its mass has not changed significantly in recent decades, the future of the East Antarctic Ice Sheet is the largest source of uncertainty in projections of future sea-level rise in a warming world. Coats Land is a region of East Antarctica that has been highlighted as potentially vulnerable to atmosphere and ocean warming, but the long-term glacial history of this area is currently poorly understood. However, the landscape hidden beneath the ice can yield valuable insights into Coats Land's deep past and how the ice sheet responds to climatic change. In this study, we use radar data to reveal the sub-ice topography of Coats Land. We identify landforms that were originally formed by tectonic activity when East Antarctica was separating from a former supercontinent approximately 150 million years ago. We also discover regions of flat topography that were formed by widespread erosion by river systems prior to Southern Hemisphere glaciation. The topography also reveals that, early in Antarctica's glacial history, regional ice flow was northward. The ice sheet subsequently reconfigured, with fast-flowing outlets draining east-to-west and ancient parts of the landscape preserved beneath non-erosive ice.

1. Introduction

The East Antarctic Ice Sheet (EAIS) is the largest reservoir of freshwater on Earth, containing an ice volume equivalent to 52.2 m of global sea-level rise (Morlighem et al., 2020). Compared to the West Antarctic Ice Sheet (WAIS), which is an order of magnitude smaller, the EAIS has not experienced a clear mass loss trend in recent decades (Otosaka et al., 2023) and has historically been viewed as less sensitive to ocean-atmosphere warming (Seroussi et al., 2020; Stokes et al., 2022; Sugden et al., 1995). However, recent work indicates that parts of the EAIS are potentially more vulnerable to climate and ocean change than previously thought. Attention has increasingly been given to the regions of the EAIS that are underlain by deep, low-lying topographic basins, which renders the ice margin potentially susceptible to rapid and irreversible retreat via marine ice-sheet

instability processes (DeConto et al., 2021; Pattyn & Morlighem, 2020). The three large-scale regions of East Antarctica that are characterized by widespread low-lying bed topography and therefore potentially vulnerable to these processes are: (a) the Wilkes Subglacial Basin, (b) the Aurora Subglacial Basin, and (c) the Coats Land sector on the eastern margin of the Weddell Sea (Golledge et al., 2017; Halberstadt et al., 2024; Morlighem et al., 2020).

Offshore sediment records and sub-ice geomorphology indicate that the EAIS margin retreated into the Wilkes and Aurora Subglacial Basins during past warm periods including Pleistocene and Pliocene interglacials, although the extent of this retreat remains uncertain (Aitken et al., 2016; Cook et al., 2013; Crotti et al., 2022). By contrast, comparatively little is known about the long-term history and dynamics of the Coats Land sector (Figure 1), largely due to the paucity of offshore sediment records in this region. Today, this area of the EAIS is drained by the combined catchment of four major outlet glaciers (the Recovery Glacier, Slessor Glacier, Bailey Ice Stream, and Stancomb-Wills Glacier) and their tributaries, which discharge into the eastern Weddell Sea (Figure 1). The catchment comprises ∼14% of Antarctica's grounded ice-sheet area (Rignot et al., 2008) and contains ∼9 m sea-level equivalent, which is more than the entire WAIS. Indeed, the Coats Land region has been identified as a likely source of major ice loss from East Antarctica during past warm climate intervals (Halberstadt et al., 2024) and over the coming centuries and millennia (Golledge et al., 2017), because ∼33% of the bed across the catchment lies below sea level (Morlighem et al., 2020) and ice at the grounding line is close to flotation (Golledge et al., 2017; Vaughan et al., 2011), which may render the catchment particularly sensitive to ocean warming.

An improved understanding of EAIS history in the Coats Land sector is crucial in order to engender greater confidence in predictions of its response to future warming. Given the paucity of offshore evidence, it is necessary to utilize alternative data sets to constrain long-term (pre- and early) glacial history. Because the subglacial landscape encodes a record of the processes that have shaped it over millions of years, the topography beneath the EAIS can be used to infer past ice dynamics (Jamieson et al., 2023; Rose et al., 2013; Ross et al., 2014). However, the sub-ice topography of Coats Land has been little studied owing to a historical lack of measurements of ice thickness (Fretwell et al., 2013). Early work used satellite imagery (from Landsat and NOAA Very High Resolution Radiometer) to map the boundaries of major physiographic zones in the ice surface (Marsh, 1985). These variations in ice-surface morphology were thought to be linked to bed topography, but the sparsity of direct ice-thickness measurements meant this could not be fully verified. More recently, a number of airborne radio-echo sounding (RES) surveys have been undertaken in this region (Corr et al., 2024; Forsberg et al., 2018; MacGregor et al., 2021; Nixdorf et al., 1999), substantially increasing the quantity and quality of available bed elevation measurements. There is therefore a significant, hitherto untapped opportunity to map and interpret the bed topography and geomorphology of Coats Land and in turn constrain the past extent, flow, and behavior of this crucial sector of the EAIS.

2. Background and Aims

2.1. Geology of Coats Land

Observations of the bedrock geology of Coats Land are limited to small rock outcrops (i.e., nunataks) across the region (Cox et al., 2023). Archean and Proterozoic basement rocks are exposed in the Shackleton Range (Will et al., 2009) (Figure 1a), where there is also evidence of fold-and-thrust tectonics dating from Gondwana assembly (ca. 550–500 Ma) (Tessensohn et al., 1999). Proterozoic granitoids are exposed in three small groups of nunataks along the Luitpold Coast (the Bertrab, Littlewood, and Moltke ("B/L/M") Nunataks; Figure 1a), although their origin remains enigmatic (Kleinschmidt & Boger, 2009). Situated between the Shackleton Range and the B/L/M Nunataks, the Theron Mountains comprise Permo–Triassic siliciclastic rocks of the Beacon Supergroup, which are intruded and/or capped by Jurassic dolerite sills of the Ferrar Large Igneous Province (Brook, 1972) (Figure 1a). Similarly, the Whichaway Nunataks to the south of the Shackleton Range comprise Ferrar dolerites that intruded into Beacon sandstones. This ca. 180 Ma tholeiitic magmatism was associated with the onset of Gondwana breakup and the separation of this sector of East Antarctica from southern Africa (Elliot, 1992).

The contrast in geology between the Shackleton Range and the Theron Mountains (to the north) and the Whichaway Nunataks (to the south) indicates that these highlands are separated by large-scale fault systems (Krohne et al., 2018). Indeed, these faults likely control the location of the Recovery and Slessor Glaciers

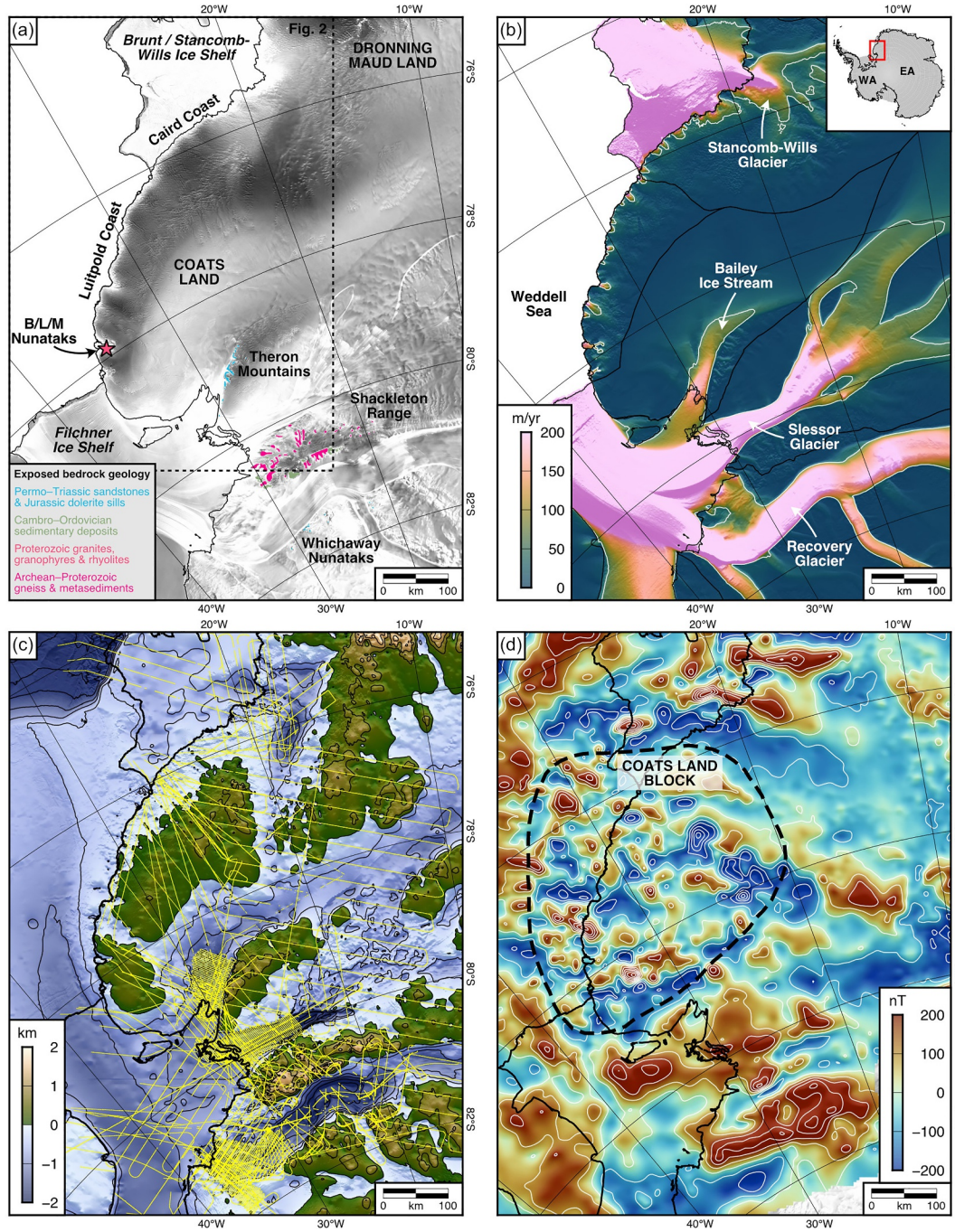

Figure 1. Geological and glaciological setting of Coats Land. (a) RADARSAT image mosaic of Antarctic ice-surface morphology (Jezek et al., 2013). Legend indicates major outcropping geological units from GeoMAP (Cox et al., 2023). B/L/M = Bertrab/Littlewood/Moltke Nunataks. Dashed box marks the extent of Figure 2. (b) MEaSUREs ice-surface velocity (Mouginot et al., 2019a). Black lines show present-day ice divides; white line demarcates the 50 m/yr contour used to illustrate the onset of fast flow. Inset shows the study area (red box) within Antarctica (EA = East Antarctica; WA = West Antarctica). (c) BedMachine v3 bed topography (Morlighem et al., 2020); contour interval is 500 m. Yellow lines mark the RES flight lines used in this study (see Figure S1 in Supporting Information S1). (d) ADMAP2B magnetic anomaly compilation (Golynsky et al., 2018); contour interval is 100 nT. Dashed black line demarcates the Coats Land Block (Jordan et al., 2017; Mieth & Jokat, 2014).

(Figure 1b), which have incised subglacial troughs with floors more than 2 km below sea level (Paxman et al., 2017; Sugden et al., 2014) (Figure 1c). Moreover, aeromagnetic anomalies support the presence of major geological lineaments bounding the Shackleton Range and reveal a magnetically distinct terrane situated between the Bailey Ice Stream and Brunt Ice Shelf, referred to as the "Coats Land Block" (Jordan et al., 2017; Mieth & Jokat, 2014) (Figure 1d). However, beyond these observations, it remains unclear to what extent the present-day subglacial geomorphology of Coats Land reflects the regional geological history and how long-term geological processes have influenced past and ongoing ice-sheet behavior.

2.2. Modern-Day Ice Dynamics

Fast ice flow in Coats Land is dominated by the Recovery and Slessor Glaciers and their tributaries (Figure 1b). These outlets are focussed through deep subglacial troughs on either side of the Shackleton Range and flow westward into the Filchner Ice Shelf, with velocities reaching 500–1,000 m/yr at the grounding line (Mouginot et al., 2019a). The Bailey Ice Stream is bounded by the northern escarpment of the Theron Mountains and also drains into the Filchner Ice Shelf but with more muted grounding-line velocities of ∼200 m/yr (Mouginot et al., 2019a). By contrast, ice surface velocities over the intervening highlands, including the Whichaway Nunataks, Shackleton Range, and Theron Mountains, are low or negligible (widely <10 m/yr; Figure 1b). To the north, the Brunt/Stancomb-Wills Ice Shelf is fed by the Stancomb-Wills Glacier, which also demarcates the eastern edge of the Coats Land Block (Figures 1b and 1d). The region bounded by the Luitpold Coast, Bailey Ice Stream, and Stancomb-Wills Glacier is characterized by predominantly slow-flowing ice, with minor glaciers with small upstream catchments present along the Luitpold Coast (Figure 1b). Evidence from internal layer stratigraphy and bed topography in the upper reaches of the Slessor and Recovery Glaciers suggests that the regional ice flow configuration has changed in the past (Diez et al., 2018; Rippin et al., 2006), but this history remains ambiguous.

2.3. Study Aims and Objectives

The overarching aim of this study is to understand the subglacial landscape of Coats Land, its evolution, and its implications for ice-sheet behavior. The objectives are threefold:

1. Map and characterize the sub-ice geomorphology of Coats Land using RES and ice-surface morphology data.
2. Elucidate the tectonic and surface processes responsible for the genesis of the modern landscape.
3. Reconstruct geological, landscape, and ice-sheet evolution and assess the implications for long-term ice-sheet behavior and sensitivity to climate change.

3. Methods

3.1. Airborne Geophysical Data Collation

3.1.1. Radio-Echo Sounding

To map the sub-ice geomorphology of Coats Land, we used bed elevation profile (i.e., 2D) data derived from RES surveying as opposed to an interpolated (3D) continental digital elevation model (DEM) such as BedMachine v3 (Morlighem et al., 2020) or Bedmap3 (Pritchard et al., 2025). The reasons for this choice were: (a) RES profile data preserve high-resolution (<5 km) detail in the landscape, which is lost during the gridding process for DEMs, and (b) in regions where ice is not fast-flowing (and therefore mass conservation cannot be used to determine ice thickness) and flight lines are widely spaced, the interpolation process can introduce artifacts that might be misinterpreted as real geomorphological features. All of our analyses were therefore performed on RES-derived bed elevation profile data, with BedMachine v3 (Morlighem et al., 2020) used solely for illustrative purposes to show the first-order regional topographic configuration (e.g., Figure 1c; Figure S2 in Supporting Information S1) and for comparison with our geomorphological mapping results.

We compiled along-track ice thickness data from four airborne RES surveys (Figure S1 and Table S1 in Supporting Information S1): (a) Alfred Wegener Institute (AWI) Dronning Maud Land (DML) (Nixdorf et al., 1999), (b) British Antarctic Survey (BAS) ICEGRAV (Forsberg et al., 2018), (c) BAS Filchner Ice Shelf System (FISS) (Corr et al., 2024), and (d) NASA Operation IceBridge (MacGregor et al., 2021). Each survey used a radar operating frequency of 150 MHz and data were processed using synthetic aperture radar (SAR) focusing (except for the AWI data). Ice thickness was determined by calculating the two-way travel time of radar reflections at the

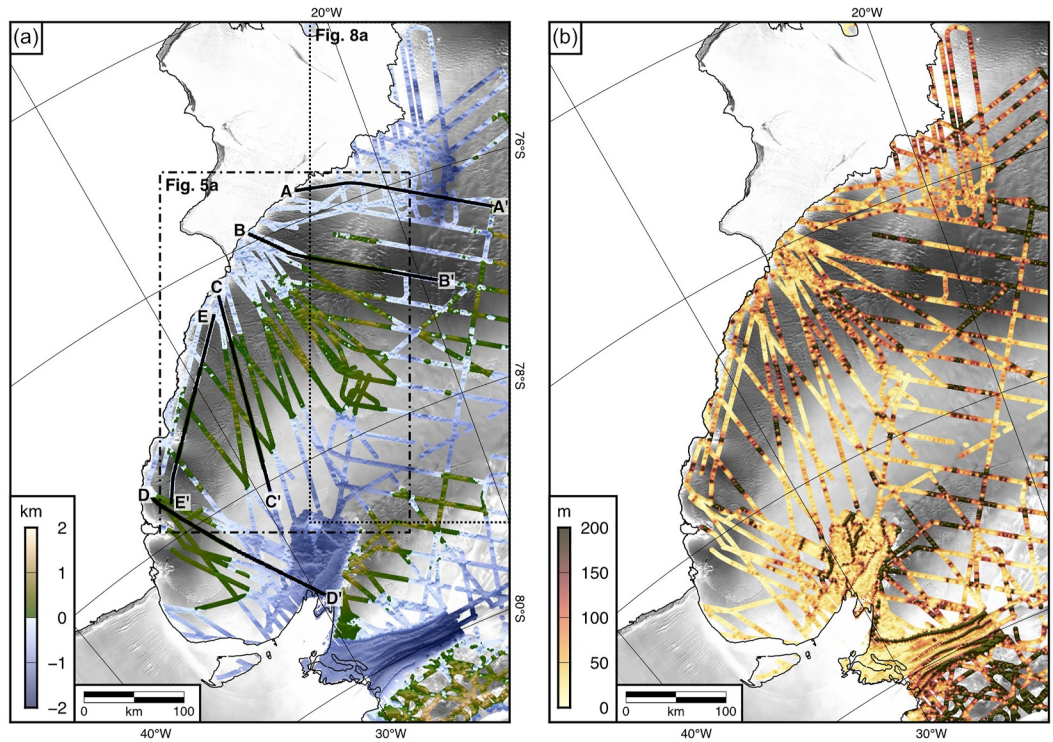

Figure 2. Coats Land sub-ice landscape derived from radio-echo sounding. (a) Bed topography. For visualization, RES-derived bed elevations were gridded at 500 m resolution and masked to remove interpolant >2,500 m from the nearest data point. Labeled lines mark the locations of profiles shown in Figure 3; dashed boxes mark the extents of Figures 5a and 8a. (b) Along-track RMS deviation of bed elevation (over a 1,600 m length scale), a proxy for local topographic roughness.

ice surface and bed interfaces. The surface and bed reflectors were picked automatically and manually corrected if necessary. Travel times were converted to depth assuming a constant radar wave speed of 0.168 m/ns, with the BAS surveys applying an additional 10 m correction for the firn layer. Ice thickness was calculated as the vertical distance between the picked surface and bed. Bed elevation (relative to the WGS84 ellipsoid) was computed by subtracting the ice thickness from the surface elevation. For consistency with continental DEMs, we shifted all bed elevation values onto the EIGEN-6C4 geoid (i.e., mean sea level; Figure 2a).

Although there were minor differences between the instrumentation and processing for each survey, the along-track bed pick data have a consistent trace spacing of 10–15 m except the older AWI data, where the spacing is ~50 m (Table S1 in Supporting Information S1). The vertical resolution is typically <10 m. Therefore, at the scale of investigation in this study (>100s of meters), differences in subglacial topography arising from differences between radar surveys are likely negligible.

3.1.2. Magnetic Anomalies

To aid geological interpretation, we also examined airborne magnetic anomalies from the 2012–2013 BAS ICEGRAV survey (other surveys have limited spatial coverage or did not acquire magnetic data). Raw total magnetic field intensity data were acquired using a Scintrex caesium magnetometer. Processing involved compensation for aircraft roll, pitch, and yaw, geomagnetic reference field correction, tip tank correction, base station correction, and compensation for heading errors (Ferraccioli et al., 2020). Since we examined only along-track line data rather than a gridded product, leveling was not required. Magnetic anomalies were collected at an approximately constant elevation relative to the WGS84 ellipsoid, a few hundred meters above the local ice surface.

3.2. Geomorphological Mapping

We systematically searched the along-track bed elevation profiles (Section 3.1.1) to map the distribution of macro-scale geomorphological features (and their boundaries) within the study area. For this mapping we primarily focussed on the region bounded by the Theron Mountains, Filchner Ice Shelf, and Brunt/Stancomb-Wills Ice Shelf; the sub-ice topography of this area has not been previously described and contains no outcrops other than the B/L/M Nunataks (Figure 1). To augment the bed elevation measurements, we derived a measure of along-track bed roughness (v) by computing the root mean square (RMS) deviation of bed elevation ($z(x)$) between points separated by a discrete length scale (Δx) of 1,600 m (Figure 2b), which is appropriate for macro-scale analysis of topography (Shepard et al., 2001):

$$v(\Delta x) = \left[\frac{1}{N}\sum_{i=1}^{N}[z(x_i) - z(x_i + \Delta x)]^2\right]^{\frac{1}{2}} \quad (1)$$

where N is the number of bed elevation measurements within the moving window (i.e., the length scale, Δx, divided by the point spacing). To ensure that RMS deviations from different RES surveys could be directly compared, all bed elevation profiles were linearly interpolated to a consistent along-track spacing of 50 m prior to the calculation. This value was chosen because it equates to the highest trace spacing of the RES surveys used (Table S1 in Supporting Information S1), minimizing the potential for aliasing or smoothing of the original data. Boundaries between macro-scale geomorphological features were delineated based on changes in regional bed elevation and RMS deviation (no specific thresholds were applied) and/or the presence of abrupt inflection points in bed slope (e.g., escarpments).

Radar survey line density varies significantly across the study area. In the lower parts of the ice streams, close to the grounding line, the FISS survey line spacing is 2.5 km. However, in the interior of Coats Land, the ICEGRAV and AWI lines are ∼25 and ∼40 km apart, respectively (Figure 1c; Figure S2 in Supporting Information S1). We therefore augmented our bed topography mapping using the 125-m-resolution RADARSAT RAMP AMM-1 SAR image mosaic of Antarctica, version 2 (Jezek et al., 2013).

The RAMP AMM-1 mosaic is a semi-quantitative representation of radar backscatter intensity, which is affected by the shape, curvature, and roughness of the ice surface. At length-scales of ∼1–20 km, undulations in ice-surface curvature (and therefore backscatter intensity) can be correlated with bed topography with wavelengths exceeding the local ice thickness (Le Brocq et al., 2008). However, backscatter variations can also arise from firn characteristics, crevassing, or aeolian features, which may exceed the influence of bed topography in certain locations. We therefore focussed this analysis on the slow-moving (∼10 m/yr; Figure 1b) interior of Coats Land, away from the grounding zone and major ice streams where crevassing is more likely (Lai et al., 2020). We used the RAMP AMM-1 mosaic to map the planform geometry of sub-ice features with wavelengths of ∼1–20 km, such as valleys, ridges, and escarpments. To ensure that the mapped backscatter features are indeed caused by the ice flowing over undulations in bed topography, we compared their positions to topographic "highs" and "lows" in intersecting RES lines.

3.3. Flexural Isostatic Modeling

Bed elevations in Antarctica have been affected by the isostatic response of the Earth's lithosphere to a number of surface and tectonic processes, including ice loading, erosion, sedimentation, volcanism, and faulting (Whitehouse et al., 2019). To gain a more complete understanding of the origin and evolution of topographic features beneath the EAIS, it is necessary to model the predicted pattern of these isostatic responses and compare these calculations to the observed topography (Paxman, 2023).

We first adjusted all RES-derived bed elevations to account for the isostatic response to the unloading of the Antarctic Ice Sheet. To do so, we used a recent calculation of the isostatic response to complete deglaciation (Paxman et al., 2022b), which was computed using a 2D flexed elastic plate model (Garcia et al., 2015), BedMachine v3 ice thickness (Morlighem et al., 2020), and a laterally variable lithospheric flexural rigidity for Antarctica (Swain & Kirby, 2021). This correction also considers the ongoing unequilibrated response of the solid Earth to Antarctic ice mass change since the Last Glacial Maximum and feedback associated with loading of areas below sea level by water.

To examine the flexural isostatic effects of other surface and tectonic processes, we used a 1D elastic plate model since the spatial geometry of these (un)loads is more difficult to constrain and opting for a simple model configuration avoids introducing additional complexity and uncertainty. The 1D equation for computing the flexure, $w(x)$, induced by a load, $h(x)$, is expressed as (Watts, 2001):

$$D\frac{d^4w}{dx^4} + \left(\rho_{\text{mantle}} - \rho_{\text{infill}}\right) g w(x) = \left(\rho_{\text{load}} - \rho_{\text{displace}}\right) g h(x) \tag{2}$$

where

$$D = \frac{E\,Te^3}{12(1-\upsilon^2)} \tag{3}$$

and the parameter Te represents the effective elastic thickness (a proxy for flexural rigidity, D) of the East Antarctic lithosphere. For simplicity, we assumed a spatially uniform Te, allowing Equation 2 to be solved analytically using a fast Fourier transform of the load and convolution with a 1D flexural isostatic response function (Watts, 2001). We assumed a Young's modulus (E) of 100 GPa, Poisson ratio (υ) of 0.25, gravitational acceleration (g) of 9.81 m s^{-2}, and mantle density (ρ_{mantle}) of 3,330 kg m^{-3}.

We computed the flexural response to three processes: (a) extensional faulting (Contreras-Reyes & Osses, 2010; Weissel & Karner, 1989), (b) glacial trough erosion (Paxman et al., 2017), and (c) continental shelf sediment deposition (Hochmuth et al., 2020). The densities of the load (ρ_{load}), the material infilling the flexure (ρ_{infill}), and the material displaced by the flexure (ρ_{displace}), as well as the distribution of $h(x)$, are dependent on the (un)loading scenario being considered. For the faulting model we tested a range of Te values, whereas for erosion and sedimentation we used a single value of 20 km, which was informed by the faulting model calculations (see Text S1 in Supporting Information S1) and represents an appropriate regional average (Swain & Kirby, 2021). The details of the (un)load geometries and densities used for each calculation are described in Text S1 in Supporting Information S1.

4. Results

In this section, we sequentially describe the first-order sub-ice geomorphological features identified through our mapping, quantify their morphology, and assess the impact of isostatic adjustment on their elevations.

4.1. Overview

RES profiles show that the bed topography of Coats Land north of the Bailey Ice Stream is dominated by terrain situated within ±500 m of present-day sea level (Figure 2a). Between the deep troughs that underlie the Bailey Ice Stream and Stancomb-Wills Glacier, the regional topography is gently inclined downwards toward the coast (Figure 3). This terrain can be divided into two first-order physiographic features: (a) low-relief planar surfaces situated close to sea level, characterized by low internal relief, and (b) a tract of high topography that rises up from the planar surfaces, including a coherent highland massif and isolated inselbergs (Figure 3). The higher topography is rougher than the adjacent planar surfaces as illustrated by its along-track RMS deviations (Figure 2b). The highlands and planar surfaces can also be clearly differentiated in the RADARSAT RAMP AMM-1 SAR image mosaic (see Section 4.2). When bed elevations are isostatically adjusted for EAIS loading, they increase by 100–400 m across the region (Figure S2 in Supporting Information S1).

The low-relief planar surfaces are bounded by the deep troughs underlying the Stancomb-Wills Glacier and Bailey Ice Stream, which are both associated with steep escarpments along their margins (Figures 4a and 4b). Additionally, several narrow (<10 km), steep-sided, topographic highs protrude from the floor of the Bailey trough with relief of up to ~300 m (Figures 4a and 4c). These flat-topped features resemble mesas located in numerous continental settings on Earth, including Antarctica (Studinger et al., 2004).

4.2. Highlands and Inselbergs

The center of Coats Land is characterized by an elongated, NE–SW-trending highland massif (Figure 4a). This belt of high terrain covers an area of ~18,000 km^2 and the peaks stand up to 800 m above the adjacent terrain. The

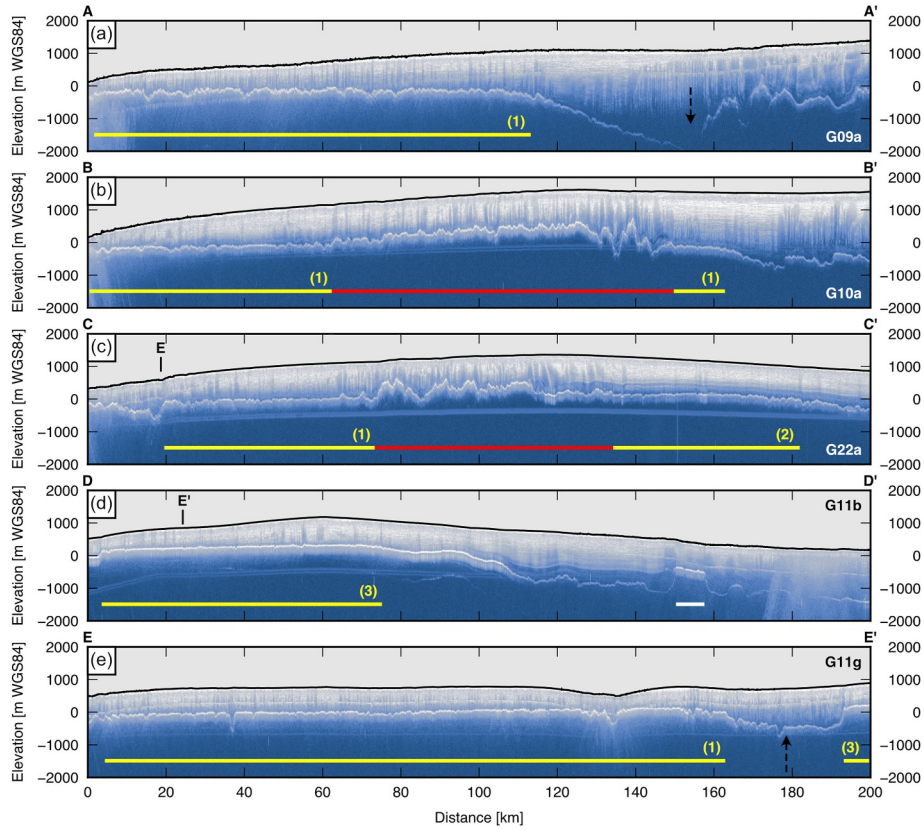

Figure 3. Radio-echo sounding images across Coats Land from the 2012–13 ICEGRAV survey. (a) Line G09a (A–A′) showing a low-relief planar surface (yellow) and an asymmetric, 40 km-wide, subglacial trough (dashed arrow). (b) Line G10a (B–B′) showing low-relief planar surfaces either side of an inclined highland massif (red). (c) Line G22a (C–C′) showing low-relief planar surfaces separated by narrower, fragmented highlands/inselbergs. (d) Line G11b (D–D′) showing a smooth planar surface and a mesa-like feature (white). (e) Line G11g (E–E′) showing an incised low-relief planar surface and a subglacial trough. Black line marks the ice surface; elevations are relative to the WGS84 ellipsoid. Numbered planar surfaces correspond to Figure 4a. All lines are oriented approximately orthogonal to the ice margin (with the margin on the left) except E–E′, which is oriented parallel to the ice margin. Projected intersection points of E–E′ with lines C–C′, and D–D′ are indicated in panels (c, d). Profile locations are shown in Figure 2a.

coastward edge trends parallel to the grounding line, which is situated 40–80 km to the northwest. The north-eastern end of the highlands (close to the Stancomb-Wills Glacier) constitutes a ∼100 km-wide, coherent massif with peak elevations up to 1.2 km above present-day sea level (when rebounded for ice unloading; Figure 4). Moving southwest toward the Filchner Ice Shelf, the highlands become lower and narrower and resemble clusters of inselbergs rather than a single massif. The topography of the highlands is rough, with a median RMS deviation of bed elevation of 120 m.

In the RAMP AMM-1 SAR image mosaic, the highlands are characterized by a more textured ice surface than the surrounding terrain (Figure 5a). The ice surface exhibits an intricate network of linear structures (Figures 5b and 5c), which resemble features that have been correlated with subglacial ridges and valleys elsewhere in Antarctica (Chang et al., 2016; Jamieson et al., 2023; Ross et al., 2014). Indeed, comparison of the location of these ice-surface lineaments with RES-derived bed elevation measurements indicates that, within the highlands, lighter areas in the surface image (greater backscatter intensity) consistently align with sub-ice ridges/peaks, whereas darker areas (lower backscatter intensity) correspond to valley floors (Figures 5b and 5c). The ridges exhibit prevailing orientations (in the EPSG:3031 Antarctic Polar Stereographic projection) of E–W and ENE–WSW (Figure 5a). Typically, the ridges proximal to the center of the highlands are oriented approximately parallel to the long axis of the elongate highland belt, whereas those closer to the edge are oriented approximately perpendicular to the boundary between the highlands and the adjacent lower terrain (Figure 5a).

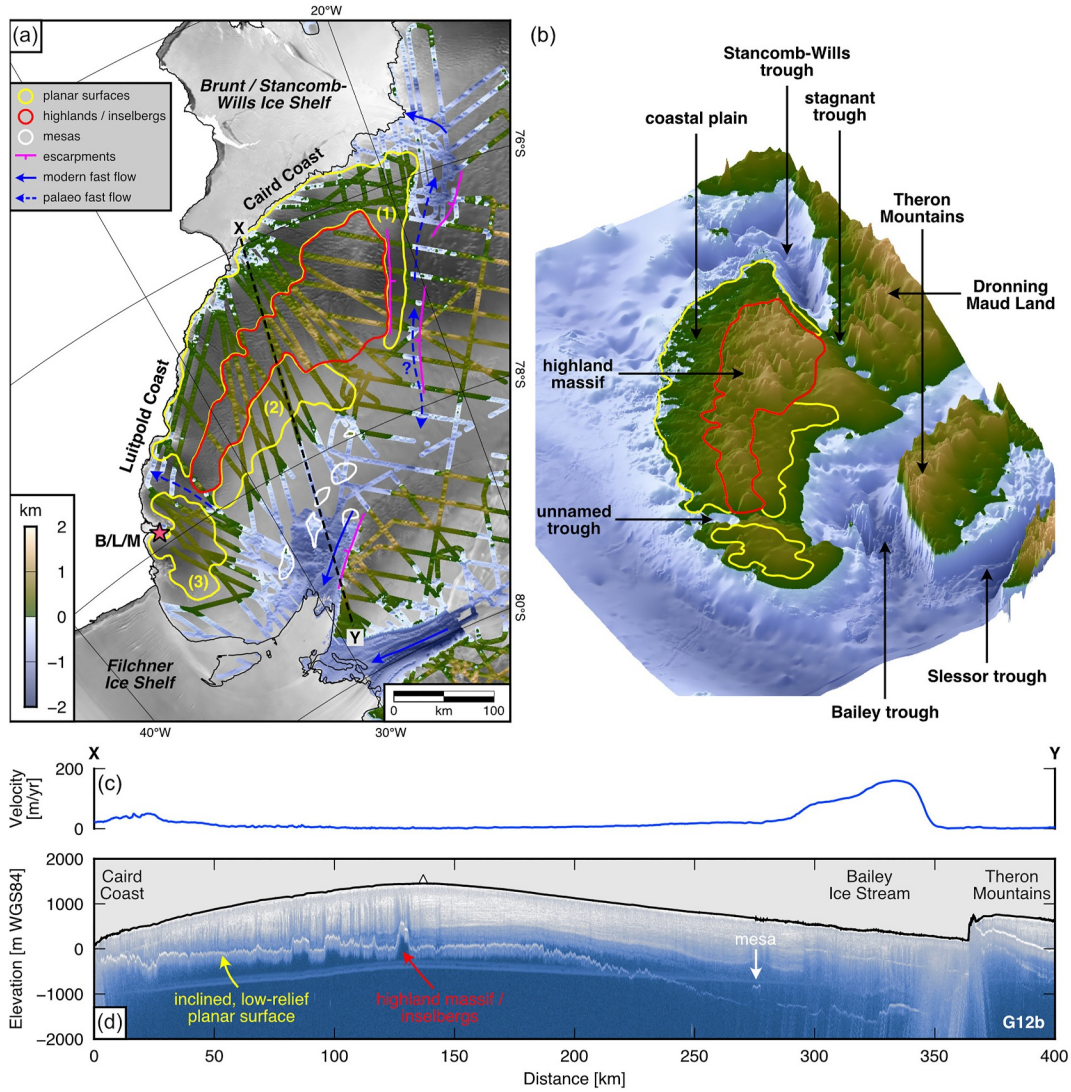

Figure 4. Geomorphological mapping of Coats Land. (a) First-order geomorphological features. RES-derived bed elevations (relative to global mean sea level) have been isostatically adjusted for EAIS removal. Outlines of geomorphological features (see legend) were mapped using RES data and the RAMP AMM-1 SAR image mosaic (backdrop). (b) Perspective image of the BedMachine v3 DEM (isostatically adjusted for EAIS unloading). The image is viewed from an azimuth of 210° and an inclination of 40°, with 40x vertical exaggeration. Color scale is the same as for panel (a). (c) Ice-surface velocity along profile X–Y (location shown in panel a). (d) Radargram along profile X–Y (ICEGRAV line G12b). Geomorphological features are labeled; black line marks the ice surface (triangle = ice divide); elevations are relative to the WGS84 ellipsoid.

Although the expressions of subglacial valleys are generally harder to distinguish than ridges, we were able to trace several features that exhibit low-order dendritic planforms (Figures 5a and 5b). Notably, the branching pattern of these valley networks implies that their downstream direction consistently faces away from the center of the highlands. We found no evidence of valleys that connect through the highlands; they instead appear to radiate from a central divide (Figure 5). Expressions of subglacial valleys within the low-relief planar surface on the coastward side of the highlands are also visible (see Section 4.3).

Elevations across the northeastern end of the highland block are strongly asymmetric. On their coastward side, the highlands rise gently up from the low-relief coastal plain, before dropping steeply by ~800 m down to the planar surface on their inland side, which separates the highlands from the Stancomb-Wills trough (Figure 6). This steep escarpment appears to coincide with a step-change in the amplitude of the magnetic anomaly (Forsberg et al., 2018) as well as the appearance of high-frequency (~5 km) magnetic anomalies over the highlands (with

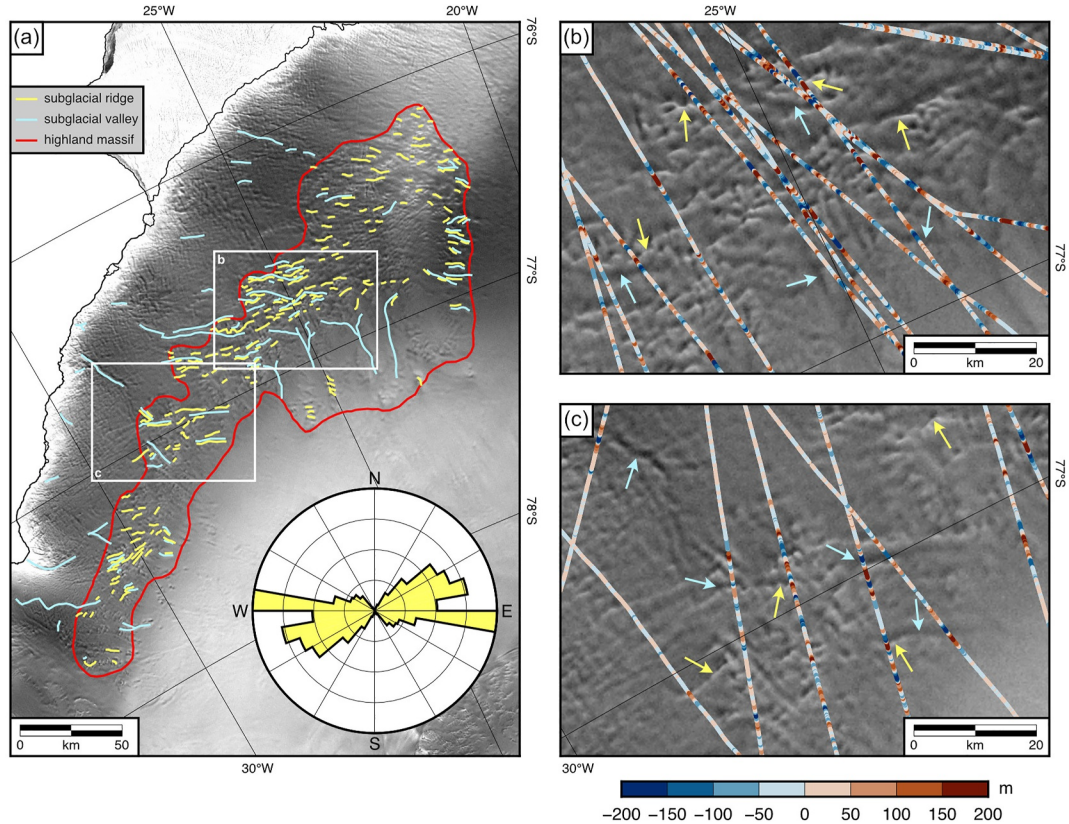

Figure 5. Ice-surface expression of subglacial ridges and valleys. (a) RADARSAT RAMP AMM-1 SAR image mosaic with mapped lineaments corresponding to subglacial ridges and valleys. Panel extent is shown in Figure 4a. Inset: polar histogram for the orientations of the mapped subglacial ridges; bin width is 10°. Ridges were assigned an orientation (in the EPSG:3031 projection) but not directionality; hence the diagram is symmetrical. (b, c) Zoom-ins of two sections of the highland massif (extents shown in panel a). Subglacial ridges are typically marked by stronger radar backscatter intensity (lighter gray) and subglacial valleys by weaker radar backscatter intensity (darker gray); see arrows for examples. Color scale illustrates the bed-elevation anomaly computed along flight tracks (observed bed elevation minus the 5-km running mean). Negative anomalies correspond to valleys and positive anomalies to peaks.

amplitudes of up to 100 nT) that are absent over the adjacent trough (Figure 6a). This transition in the magnetic anomaly is indicative of the presence of a geological boundary, such as a fault system and/or a change in lithology.

This hypothesis is further supported by 1D flexural modeling (Text S1 in Supporting Information S1), which shows that the mechanical unloading induced by displacement across a normal (i.e., extensional) fault produces a predicted pattern of uplift that is consistent with the observed first-order geometry of the highland block (Figure 6b; Figure S3 in Supporting Information S1). Specifically, the model predicts a steep escarpment proximal to the locus of the unloading (i.e., the fault), with the uplift profile tilting gently downwards moving away from the fault. The amplitude of the escarpment and the westward tilt of the block are best fit by a model with a faulted layer depth of 28 km (Figures 6b and 6c), which is consistent with values inferred for "cold" continental rifts associated with cratonic lithosphere and/or low heat flow, such as the Baikal Rift or parts of the East African Rift (Chen & Molnar, 1983; Lavier & Buck, 2002). The best-fitting *Te* of 21 km (Figures 6c and 6d) is in good agreement with previous estimates from the Shackleton Range (Paxman et al., 2017) and regional values derived from inverse spectral analysis of gravity anomalies and topography (Swain & Kirby, 2021). Notably, the model overpredicts the elevation of the low-relief coastal plain on the coastward side of the highlands (Figure 6b). This indicates that at least one additional process is required to explain the current elevation of this surface (see Section 5), which is delineated from the highlands by a ~200–300 m "step."

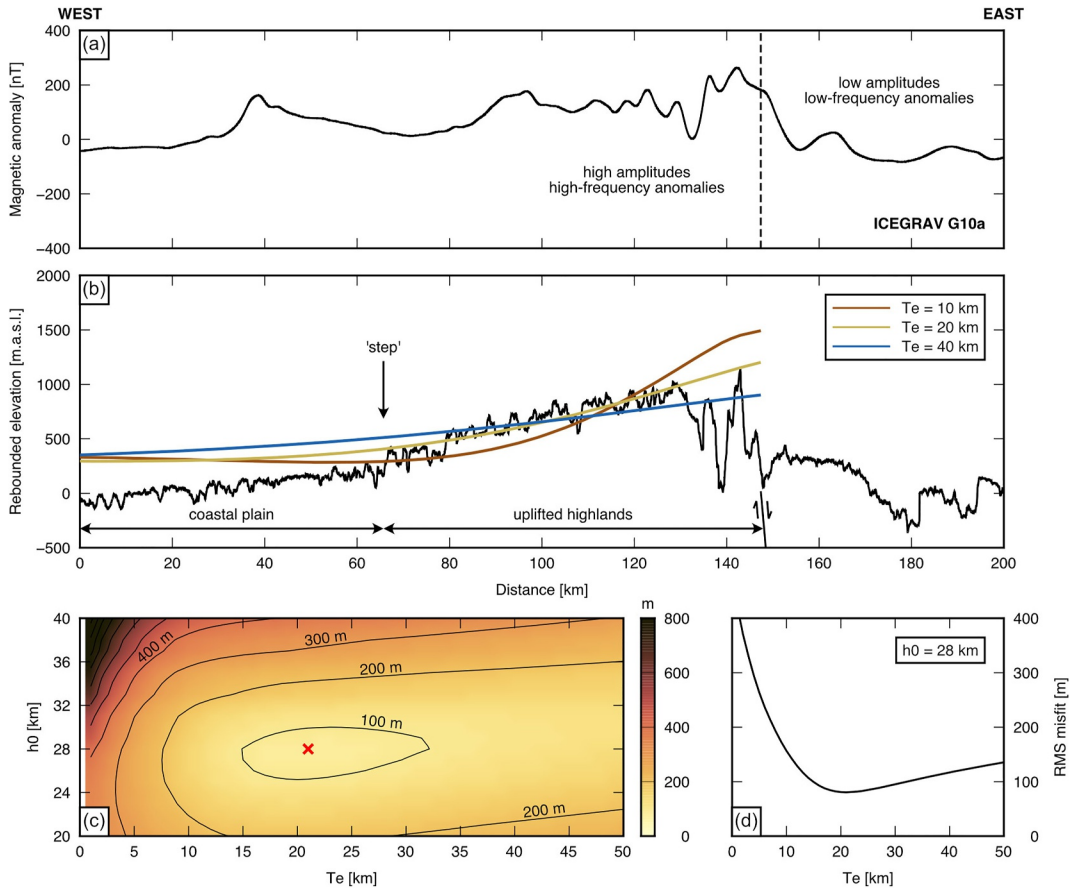

Figure 6. Flexural response to mechanical unloading. (a) Magnetic anomaly along ICEGRAV line G10a (profile B–B′ in Figure 2a). Vertical dashed line marks the location of a transition in magnetic character (anomaly amplitude and frequency). (b) Bed topography along G10a. Black line illustrates the modern bed topography, isostatically adjusted for the removal of the present-day ice-sheet load (Paxman et al., 2022b); colored lines show the flexural uplift profiles computed using a 1D broken elastic plate model. The flexure is caused by mechanical unloading along a normal fault (plate break) bounding the eastern margin of the highlands (location shown in panel b, corresponding to the magnetic anomaly transition in panel a). Profiles are shown for three effective elastic thickness (*Te*) values for the lithospheric plate. (c) RMS misfit between the modeled and observed bed topography across the highland block as a function of *Te* and faulted layer depth (*h*0). The red cross marks the best-fitting combination; $Te = 21$ km and $h0 = 28$ km. (d) RMS misfit as a function of *Te* for a constant *h*0 of 28 km. The flexural model can account for the steep eastern escarpment and westward tilt of the highland block but overpredicts the coastal plain (0–65 profile-km) elevation by ~200–300 m.

4.3. Low-Relief Planar Surfaces

The most conspicuous features in the RES profiles that image the Coats Land bed are the extensive low-relief planar surfaces that exhibit consistent elevations over distances of tens to hundreds of kilometers (Figure 3). Based on the distribution of these features in the RES profiles and augmented by RADARSAT imagery, we mapped three distinct contiguous planar surfaces within the study area (Figure 7a). These three surfaces can be distinguished from the highlands (Section 4.2) based on their median RMS deviations of bed elevation, which are 49, 25, and 20 m (compared to 120 m in the highlands).

Planar surface 1 (hereafter "PS1") covers ~22,000 km^2 and borders the coastward side of the highland block (Section 4.2) on one side and the Luitpold Coast on the other. It is 40–80 km wide and extends laterally for ~350 km. PS1 "wraps" around the northeastern end of the highlands, forming a ~20 km-wide tract of flat terrain between the highlands and the Stancomb-Wills trough (Figure 7a). The surface is characterized by coherent top elevations and short-wavelength (<10 km) roughness (resulting in a median RMS deviation of 49 m; Figure 2b) in the form of narrow, steep-sided valleys (Figures 3a, 3b, and 3e). The depth of these valleys tends to increase moving toward the grounding line, with some features incised 500 m into the flat-topped surface. The floors of

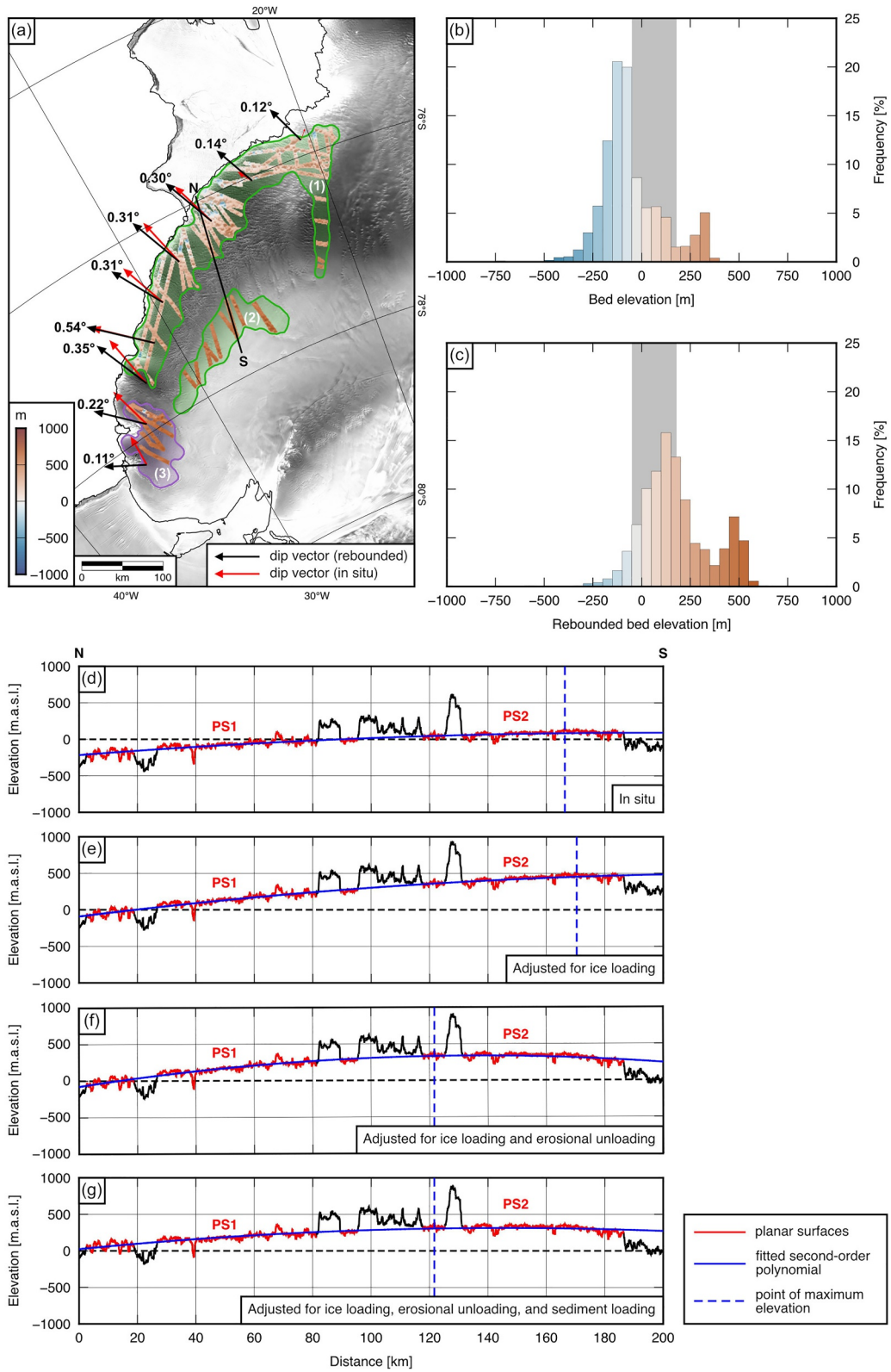

Figure 7.

these valleys are as deep as ~500 m below sea level (~300 m when adjusted for ice-sheet unloading). The planforms of some of these valleys can also be traced in the RAMP AMM-1 SAR image mosaic (Figure 5a).

Planar surface 2 ("PS2") covers ~6,700 km^2 and is located between the inland limit of the highlands and the point where the terrain drops down into the Bailey trough (Figures 3c and 4d). The roughness of PS2 (median RMS deviation of 25 m) is lower than PS1, primarily because deeper valleys are largely absent. PS2 is 20–40 km wide and ~150 km long, extending northeastward from the southwestern end of the highlands; together, PS1 and PS2 do not completely enclose the highland block (Figure 7a).

Planar surface 3 ("PS3") covers ~4,800 km^2 and is located southwest of the other two surfaces and the highlands, separated by an unnamed, 40 km-wide, U-shaped trough (Figure 3e). PS3 is characterized by particularly smooth bed topography (median RMS deviation of 20 m), which is almost completely devoid of small-scale roughness or valley incision (Figure 3d).

Hypsometric analysis reveals that the elevations of the planar surfaces are highly clustered. At the present-day (i.e., beneath the EAIS), the modal RES-derived elevation across the surfaces is 50–150 m below sea level, with a smaller hypsometric peak at ~300 m above sea level corresponding to parts of PS2 (Figure 7b). When these elevations are adjusted for ice-sheet unloading, the position of the main hypsometric peak widens and shifts to 0–250 m above sea level (Figure 7c), again with a smaller subsidiary peak at ~500 m above sea level.

We also determined the dip and dip direction of the coast-adjacent surfaces (PS1 and PS3) by fitting a linear plane (by least-squares regression) to the bed elevation measurements within a 100 × 100 km moving window. This calculation was performed for both the observed (in situ) and rebounded (ice-free) bed elevation measurements. We found that rebounding the planar surfaces for ice unloading caused their dips to: (a) become steeper, (b) exhibit more consistent magnitudes (0.1–0.5°), and (c) become more consistently oriented orthogonal to the coast (Figure 7a). This implies that PS1/2/3 are fragments of a single surface, suggesting that the surfaces were originally formed using a common process before their morphologies subsequently diverged.

We note that the planar surfaces may also have been vertically displaced processes other than ice-sheet loading. Specifically, it is likely that surface elevations will have been impacted by the flexural response to: (a) incision of the nearby glacial troughs, and (b) deposition of glacial sediments on the adjacent continental shelf (see Text S1 and Figure S4 in Supporting Information S1). When the planar surface elevations are adjusted solely for ice loading, both PS1 and PS2 dip in an offshore direction (i.e., northwestward; Figure 7d). However, when these elevations are further adjusted to remove the effect of erosional unloading, we find that PS2 (i.e., closer to the locus of glacial incision in the Bailey trough) is lowered by ~200 m and becomes near-horizontal or reversed to a gentle inland slope (Figure 7e). The flexural response to erosional unloading has a more muted impact on PS1 (i.e., closer to the coast). However, with an additional adjustment for offshore sediment loading, the near-coastal surfaces are elevated by ~100 m (Figure 7f). Therefore, accounting for the flexural responses to glacial erosion and sedimentation changes the overall pattern of tilts, such that PS1 and PS2 dip (more gently) in opposite directions on either side of the highlands (Figure 7g).

4.4. Mesas

We also mapped six isolated, steep-sided, flat-topped topographic highs situated close to the Theron Mountains (Figure 4a). These features are typically <10 km wide and characterized by steep walls and flat tops (e.g., Figures 3d and 4d); their prominence is typically ~300 m. As well as being conspicuous in radar images, the extent of these surfaces is visible in the RAMP AMM-1 SAR image mosaic, owing to their steep sides producing a clear inflection in bed and surface curvature. The six features, which resemble mesa/butte topography, form a NE–SW-

Figure 7. Geometry of the low-relief planar surfaces. (a) Distribution of low-relief planar surfaces in RES survey lines. Elevations have been isostatically adjusted for removal of the modern EAIS (Paxman et al., 2022b). Vectors indicate the dip directions of a linear plane fitted by least-squares regression to bed elevation data (red = in situ; black = rebounded) within a 100 × 100 km window moving around the coast. Vector lengths are logarithmically scaled to the labeled dip angles. Three separate planar surfaces are divided into two morphological groups: PS1 and PS2 (green), and PS3 (purple). (b) Hypsometry (frequency distribution of elevations; 50 m bins) of the planar surfaces using in situ bed elevation measurements. (c) Hypsometry using bed elevations rebounded for ice-sheet unloading. Gray region indicates the range of Cenozoic (66–0 Ma) global mean sea level, smoothed over an 800 kyr window (Miller et al., 2024). (d) Present-day bed elevation profile along ICEGRAV line G12b (see Figure 4d). (e) Profile adjusted for the removal of the modern ice-sheet load (Paxman et al., 2022b). (f) Profile adjusted for ice loading and (glacial) erosional unloading. (g) Profile adjusted for ice loading, erosional unloading, and sediment loading.

trending chain immediately adjacent to the margin of the fast-flowing Bailey Ice Stream. Fast ice flow is confined to the 30–40 km-wide region between these mesa-like features and the Theron Mountains.

4.5. Subglacial Troughs

Our mapping also revealed three major subglacial troughs within the study area. The trough underlying the Bailey Ice Stream separates the highlands, planar surfaces, and mesas described in Sections 4.2–4.4 from the Theron Mountains. The trough is 30–50 km wide, with a well-defined southern margin comprising a 2 km-high escarpment that forms the edge of the Theron Mountains block (Figure 4d). The shape of the trough is strongly asymmetric, with a gentler slope on the northern side of the ice stream. Although not always clearly imaged by RES, the floor of the trough is ∼1.5 km below sea level (Figure 4d).

The trough underlying the Stancomb-Wills Glacier separates the Coats Land highlands from the westernmost end of the Dronning Maud Land mountain chain (Figure 4b). This trough is also ∼50 km wide and the cross-sectional profile is highly asymmetric, with one side characterized by a gently sloping margin and the other by a steep, ∼2 km-high escarpment (Figure 8). The terrain immediately southeast of the Stancomb-Wills trough is characterized by rough topography with sharp ridges and U-shaped valleys that appear to "feed into" the main trough (Figures 8c and 8d). The deepest parts of the Stancomb-Wills trough are ∼2 km below sea level. Moreover, the Bailey and Stancomb-Wills troughs are connected by a ∼20 km-wide channel with a floor ∼1 km below sea level (Figure 8b). In the BedMachine v3 DEM, this trough is characterized by a "chain" of enclosed topographic lows corresponding to the crossing points of the RES lines (Figure 8b). The unrealistic topographic highs in between are interpolation artifacts, highlighting the importance of interpreting geomorphology from the radar lines, which can facilitate the construction of more realistic topographic grids. This demonstrates an important limitation of BedMachine, which cannot reliably derive bed elevation in areas lacking in fast-flowing ice (i.e., mass conservation cannot be applied) and dense RES survey coverage. This is particularly pertinent for troughs not presently occupied by fast-flowing ice, such as those in this part of Coats Land.

A third (unnamed) trough is present at the southwestern end of the highlands. This U-shaped feature is up to ∼40 km wide but is shallower than the Bailey and Stancomb-Wills troughs, with a floor ∼500 m below sea level (Figure 3e). It separates the smooth PS3 from the rougher PS1 and PS2 (Figure 4a) and is oriented perpendicular to the coast. Modern ice-surface velocities within this trough are low (Mouginot et al., 2019a) and the internal layers within the ice column appear to be conformable and undisturbed (Figure 3e).

5. Discussion

In this section, we discuss the implications of our results for the geological history of Coats Land, how this preconditioned the pre-glacial landscape and early ice growth, and how the landscape influenced and recorded subsequent EAIS evolution.

5.1. Geological History

The low-relief planar surfaces and intervening highlands have zero surface exposure, which makes it challenging to constrain their lithology. However, PS3 is situated beneath ice immediately adjacent to the B/L/M Nunataks (Figure 4a), which comprise Mesoproterozoic (ca. 1.1 Ga) granites, granophyres, and rhyolites (Cox et al., 2023). Moreover, aeromagnetic anomalies reveal that the region containing the B/L/M Nunataks and the planar surfaces and highlands mapped in this study constitutes a magnetically coherent geological province (Figure 1d) distinct from the surrounding terrain and most likely cratonic in nature (Jordan et al., 2017; Mieth & Jokat, 2014; Studinger & Miller, 1999). We therefore assume that these topographic features are predominantly composed of Proterozoic basement rocks.

Our results indicate that Coats Land experienced a period of regional extensional tectonic deformation prior to EAIS inception. The evidence for this is threefold. First, the deep, asymmetric profiles of the troughs underlying the Bailey Ice Stream and Stancomb-Wills Glacier (Figures 4d and 8b) are reminiscent of half-graben basins commonly found in extensional regions elsewhere on Earth (Buck, 1991). Second, the steep escarpment and tilted flank of the subglacial highlands to the west of the Stancomb-Wills trough are consistent with flexural uplift caused by normal faulting (Figure 6b); this topography is mirrored by the Theron Mountains on the edge of the Bailey trough (Figure 4d) (Paxman et al., 2017). The proposed location of the fault system along the Stancomb-

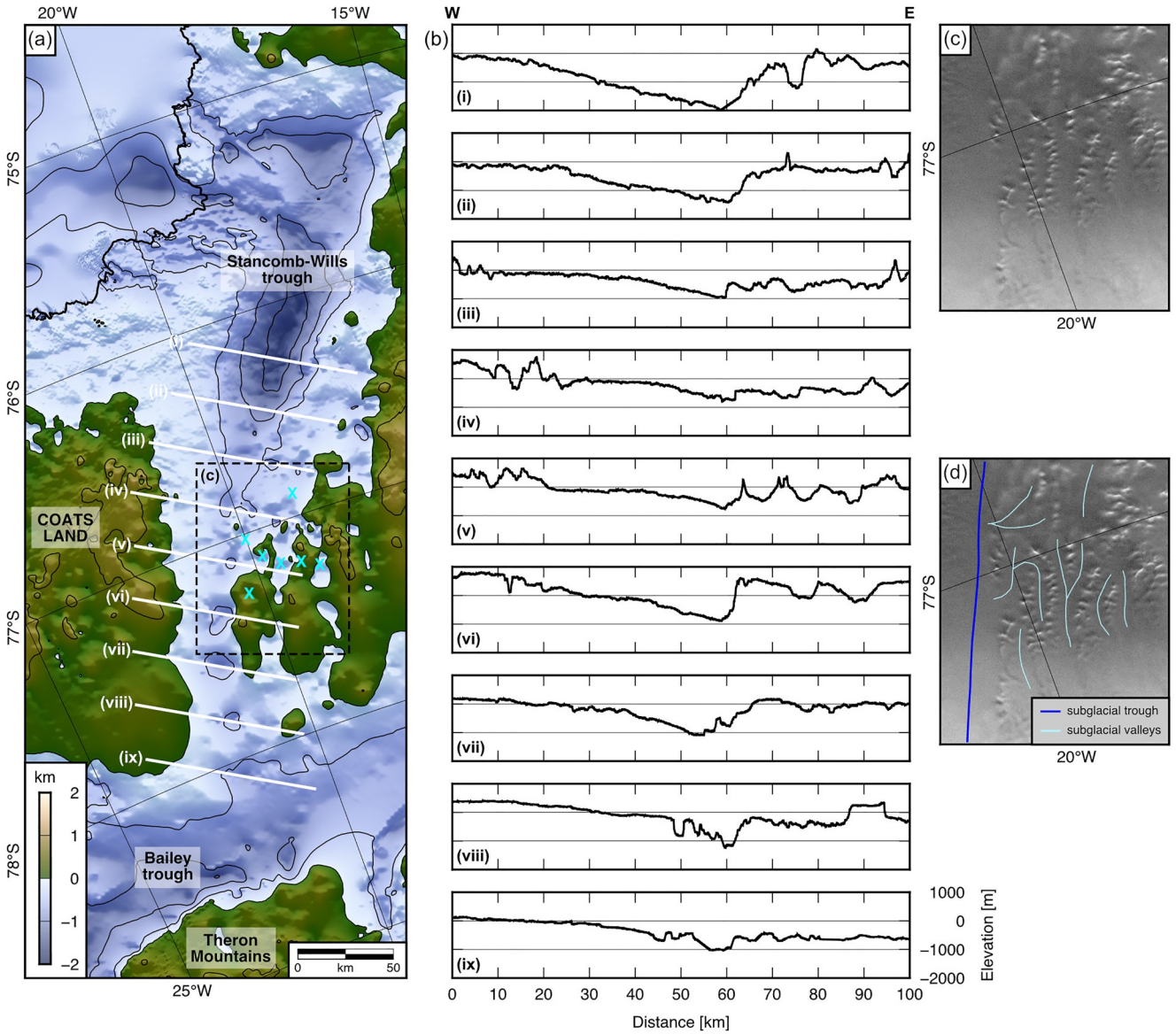

Figure 8. Geometry of the trough bounding the eastern margin of Coats Land. (a) Map of the region between the Stancomb-Wills and Bailey glacial troughs. Panel extent is shown in Figure 4a. Bed elevation from BedMachine v3 (Morlighem et al., 2020); contour interval is 500 m. Thick black line marks the present-day grounding line; white lines mark the locations of the profiles (i–ix) shown in panel b; dashed box marks the extent of panels (c, d). (b) RES-derived bed elevation profiles crossing the subglacial channel that connects the Stancomb-Wills and Bailey glacial troughs. The profiles are stacked from north (i) to south (ix) and oriented from west to east. Elevations are relative to the global mean sea level. Note that the trough floor is shallowest in profile v (~77°S) and progressively deepens to the south and north. Each profile is from the 2012–13 ICEGRAV survey (i = G09a; ii = G09a; iii = G02b; iv = G10a; v = H03b; vi = H03b; vii = G07a; viii = G07a; ix = G04d). (c) RADARSAT RAMP AMM-1 ice-surface morphology image of the region outlined by the dashed box in panel (a). (d) Interpreted version of the RADARSAT RAMP AMM-1 image. Profile v shows that this area exhibits sharp ridges and U-shaped valleys with floors sitting above that of the neighboring trough. Locations of subglacial valleys are shown in panel a (blue crosses).

Wills trough also coincides with a pronounced change in the amplitude and frequency content of the magnetic anomaly (Figure 6a), which is indicative of the presence of a geological boundary. Third, the topographic mesas within and adjacent to the Bailey trough (e.g., Figure 3d) resemble landforms that are strongly associated with Ferrar tholeiitic intrusions in East Antarctica (Studinger et al., 2004). These rocks are exposed in the neighboring Theron Mountains (Figure 1a), which exhibit similar mesa topography (Paxman et al., 2017), making it highly probable that the subglacial mesas reflect the presence of the same intrusive sequences. The Ferrar intrusions were emplaced during early Jurassic extension associated with Gondwana breakup (Elliot, 1992).

The early Jurassic (ca. 180 Ma) is the most recent period characterized by widespread crustal extension and magmatism in the eastern Weddell Sea region (Jordan et al., 2013; Riley et al., 2020). Moreover, Jurassic extension has been recognized in Dronning Maud Land, where the Jutulstraumen Graben has been imaged (Ferraccioli et al., 2005). This extension was associated with the separation of East Gondwana (India, Australia, and Antarctica) from West Gondwana (South America and Africa). The age of the oceanic lithosphere indicates that a seaway had begun to form between East Antarctica (Coats Land/Dronning Maud Land) and its conjugate margin in southern Africa by ca. 150 Ma (Müller et al., 2016). We propose that the large-scale subglacial troughs (Stancomb-Wills and Bailey) and associated escarpments and tilted highlands in Coats Land were most likely formed during this phase of early Jurassic rifting and Gondwana breakup (Figure 9a). This proposed timing is supported by: (a) the exposure of Ferrar tholeiites in the Theron Mountains and the presence of morphologically similar mesas within the Bailey trough, and (b) thermochronological data and thermal history modeling that indicate the nearby Shackleton Range experienced substantial crustal heating in the Jurassic (Krohne et al., 2018). We suggest that Jurassic extensional deformation may have exploited inherited geological weaknesses (Ferraccioli et al., 2005) and/or been focussed in more mobile belts around the edges of cratonic terranes such as the Coats Land Block (Jordan et al., 2017; Mieth & Jokat, 2014). However, we cannot entirely discount the possibility of extensional deformation occurring earlier, for example, during Permo-Triassic rifting that affected other parts of East Antarctica (Ferraccioli et al., 2011; Maritati et al., 2020).

Half-graben basins formed during extension in Coats Land would likely have acted as depocentres that were filled with sediments. Indeed, geophysical observations support the presence of a 3 km-thick fault-bounded sedimentary basin beneath an upstream tributary of the Slessor Glacier (Bamber et al., 2006), indicating that extension occurred in this region, which is topographically connected to the Stancomb-Wills and Bailey troughs. We suggest that sediments filling the Stancomb-Wills and Bailey troughs may have been at least partially eroded by the EAIS (Section 5.3). This would account for their characteristic half-graben morphology (Figure 8) being better preserved than in many extinct sediment-filled rift systems elsewhere on Earth (Maritati et al., 2020).

5.2. Pre-Glacial Landscape and Early Ice Growth

The correlation between RES bed elevation measurements and undulations in the RAMP AMM-1 SAR image mosaic shows that the Coats Land highlands contain a network of ridges and valleys. The branching, dendritic nature of the valley planforms and intricacy of the ridge-and-valley networks indicate that the highlands were initially incised by fluvial systems, with flow radiating away from the center of the highlands (Figure 5a). We therefore suggest that these are one of several examples of subglacial highlands where elements of a pre-glacial fluvial valley network have been preserved beneath the EAIS since ca. 34 Ma (Franke et al., 2021; Jamieson et al., 2023; Rose et al., 2013). RES profiles also show that across much of the highlands the valleys are relatively shallow (<300 m), narrow (<2 km) and V-shaped (Figures 3b and 3c), as would be expected for fluvial systems. However, this does not preclude a degree of later modification by glacial incision (see Section 5.3).

The low-relief planar surfaces are also likely to be erosional features that post-date highland uplift; we suggest that they originated as pre-glacial fluvial planation surfaces. The reasons for this are threefold. First, the clustering of the ice-free elevations of the surfaces around a single modal peak close to sea level (Figure 7c) is indicative of widespread planation to a former base level. Second, the ice-free surface systematically dips coastwards at low angles (<0.6°; Figure 7a), consistent with coastal plains formed by fluvial planation along former Gondwanan passive margins, including southern Africa (Cockburn et al., 2000). Third, the topographic "step" on the coastward side of the highlands (Figure 6b) resembles a small escarpment formed by backwearing as fluvial systems erode the landscape down to base level; this would account for PS1 being 200–300 m lower than predicted by the flexure model (Figure 6b). Notably, flat topographic surfaces interpreted as having formed via fluvial planation are also preserved further west around the Weddell Sea Embayment (Carter et al., 2024; Rose et al., 2015) and around other parts of the East Antarctic margin (Paxman, Jamieson, et al., 2025).

We discount both marine and ice-sheet planation as primary formation mechanisms for the planar surfaces as there are no modern analogs for the generation of coherent, morphologically consistent erosion surfaces extending tens of kilometers inland over lateral distances of hundreds of kilometers via these processes. By contrast, fluvial planation commonly forms low-elevation, gently dipping coastal plains, which represent the erosive response of the landscape to a change in base level (Braun, 2018). A consequence of early Jurassic rifting and the creation of a seaway between East Antarctica and southern Africa would have been the establishment of a

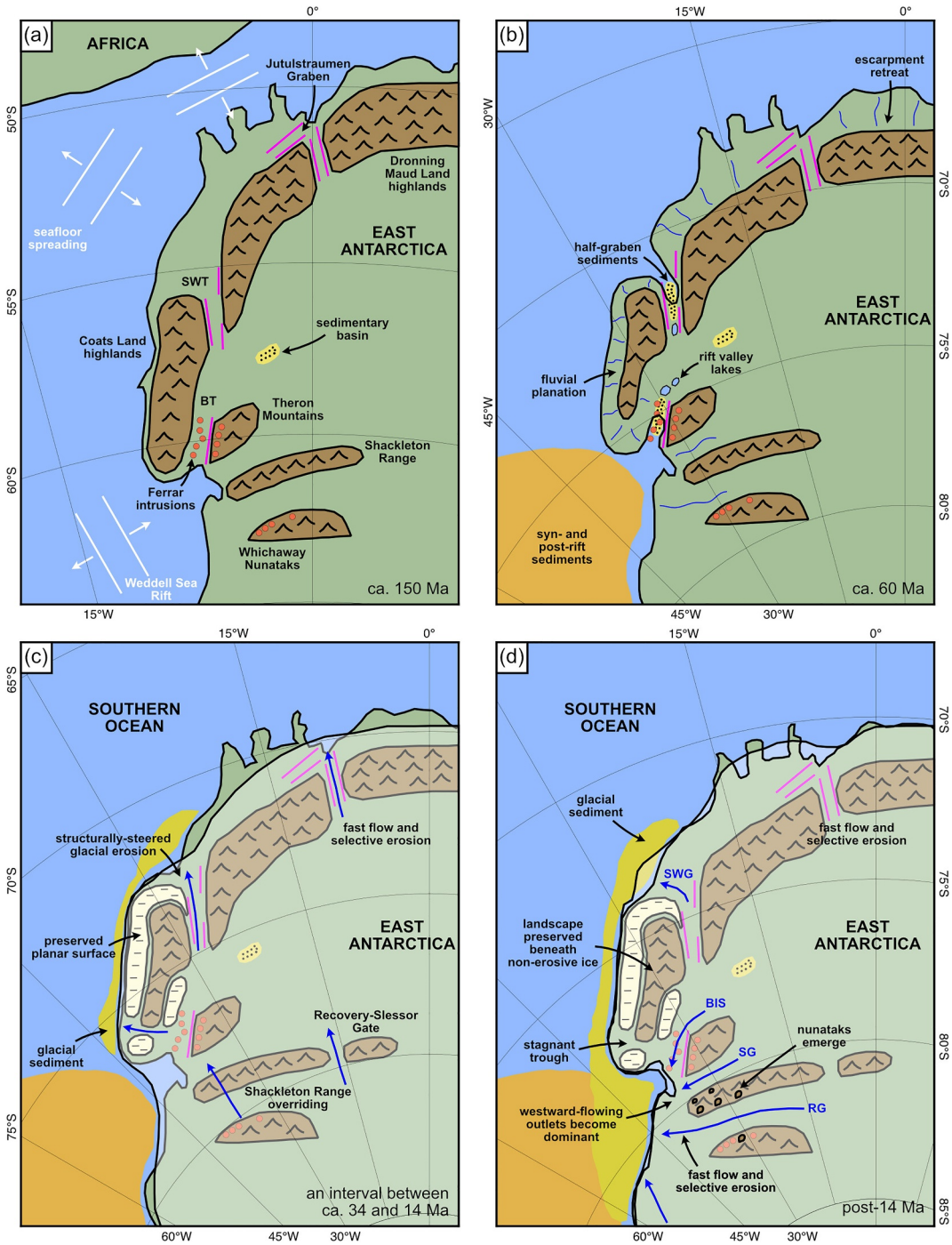

Figure 9. Schematic landscape evolution model for Coats Land. (a) The Jurassic period was associated with seafloor spreading between Africa and East Antarctica (ca. 150 Ma) (Müller et al., 2016) and Weddell Sea rifting (Jordan et al., 2013). In Coats Land, this period of extension was associated with the development of half-graben basins (Bamber et al., 2006), highland uplift, and Ferrar dolerite emplacement (Elliot, 1992). BT = Bailey trough; SWT = Stancomb-Wills trough. (b) By the early Cenozoic (ca. 60 Ma), fluvial systems had eroded a coastal plain down to sea level, with the edge of the highlands retreating inland. The now-inactive extensional basins were likely associated with shallow marine embayments, lakes, and/or sedimentary infill. (c) After a short period of alpine glaciation in the highlands, fast-flowing ice exploited the inherited rift structures and selectively eroded deep troughs during an early phase of glacial expansion (pre-14 Ma). Regional ice flow was south-to-north, with warm-based ice overriding the Shackleton Range (Sugden et al., 2014). (d) Following the mid-Miocene climate transition expansion at ca. 14 Ma, the Recovery and Slessor glacier systems became dominant with ice flow switching east-to-west. Ice in Coats Land became predominantly slow-flowing and cold-based, preserving the now-stagnant troughs and pre-glacial topography.

new (lower) base level in a region previously situated within the Gondwanan supercontinent. Fluvial systems would have responded by eroding the new coastal regions to the sea level, with a knickpoint (i.e., topographic "step" coinciding with a change of gradient) forming at the coast and propagating inland via headward erosion (Figure 9b). Indeed, the coastal planation surface elevations (100–200 m above sea level when adjusted for ice loading, erosion, and sedimentation) broadly align with early Cenozoic global sea levels (Figure 7) (Miller et al., 2024).

Today, the topographic "step" and change of gradient are observed ~60–80 km inland of the coast (Figure 6b). Approximately 120 million years elapsed between seafloor spreading onset and glaciation, implying a long-term average retreat rate of ~0.5–0.7 km Myr^{-1}. This is comparable to rates inferred from passive margin escarpments elsewhere on Earth (Braun, 2018). A corollary of this scenario is that the width of the highland block would have initially been greater than today (as predicted by the flexure model; Figure 6b) but was reduced (and divided into inselbergs toward the southwest; Figure 4d) by fluvial downwearing and backwearing of the landscape (Figure 9b).

Although PS2 (on the inland side of the highlands) is coastward-dipping at the present-day (Figure 7d), adjusting for the flexural effects of glacial erosion and sedimentation suggests that, prior to glaciation, PS2 was flat-lying or dipped gently in the opposite direction to PS1 (Figures 7f and 7g). This implies that PS2 was eroded to a different base level on the inland side of the highlands. We suggest that in pre-glacial times the "extensional corridor" represented by the Stancomb-Wills and Bailey half-graben basins would have been low-lying, and most likely characterized by either: (a) shallow marine embayments or (b) enclosed lake-filled rift valleys. Both scenarios would have provided a local base level for fluvial systems accounting for PS2 formation. We therefore suggest that between separation from southern Africa (ca. 150 Ma) and glacial inception (ca. 34 Ma), the topography of Coats Land began to resemble present-day Madagascar (Sugden & Jamieson, 2018), with coastward-dipping fluvial plains either side of a central highland massif. We note however that because PS1 and PS2 do not fully enclose the highlands, the Stancomb-Wills and Bailey embayments likely did not connect at this time (i.e., Coats Land was a peninsula rather than an island; Figure 9b).

5.3. Ice-Sheet History

In Sections 5.1 and 5.2, we proposed that the first-order physiographic features of the Coats Land landscape were originally formed in pre-glacial times. One exception is that, in parts of the highlands, steep-sided U-shaped valleys separated by sharp ridges (Figures 3b, 8b, and 8d) are indicative of erosion by valley glaciers. We surmise that the original fluvial network (Section 5.2) was locally exploited and overprinted by highland ice masses during the early stages of glaciation in this region. However, landscape modification was not as extensive or intensive as in other parts of East Antarctica, such as Dronning Maud Land, the Gamburtsev Subglacial Mountains, and the Transantarctic Mountains, where more dramatic mountain glacial topography is observed (Barr et al., 2022; Franke et al., 2021; Rose et al., 2013). We attribute this difference to the lower altitude, lower latitude, and/or more coastal setting (i.e., warmer temperatures) of Coats Land relative to these regions, meaning that mountain glaciation likely commenced later and was relatively short-lived before a continental-scale ice sheet coalesced (DeConto & Pollard, 2003; Jamieson et al., 2010).

The finding that the Coats Land highlands and planar surfaces constitute a preserved landscape that has survived beneath the EAIS with limited modification since ca. 34 Ma has important implications for past ice-sheet behavior. This indicates that long-term average glacial erosion rates across Coats Land have been markedly low, which we attribute to the persistence of slow-moving, cold-based ice. Indeed, contemporary ice-surface velocities are low across the planar surfaces and highlands (Mouginot et al., 2019a) (Figure 10a) and modeled basal temperatures are widely >8°C below the pressure melting point (PMP) (Dawson et al., 2022) (Figure 10c). Our findings indicate that these conditions have likely prevailed over these higher elevation parts of Coats Land for the majority of the time since the establishment of a continental-scale EAIS at ca. 34 Ma.

However, some of the valleys within PS1 must have been incised by ice (e.g., fjord-terminating glaciers) or subglacial meltwater, since their floors are up to 500 m below sea level (Figure 3e). These valleys (Figure 5a) coincide with the positions of modeled subglacial hydrological drainage channels (Figure 10d) and basal ice that is modeled to be within 2°C of the PMP at the coast (Figure 10c) (Dawson et al., 2022). We therefore suggest that episodes of relatively modest basal warming could have induced the localized formation of these subglacial valleys, while preserving the larger-scale structure of the inherited fluvial planation surface into which they are

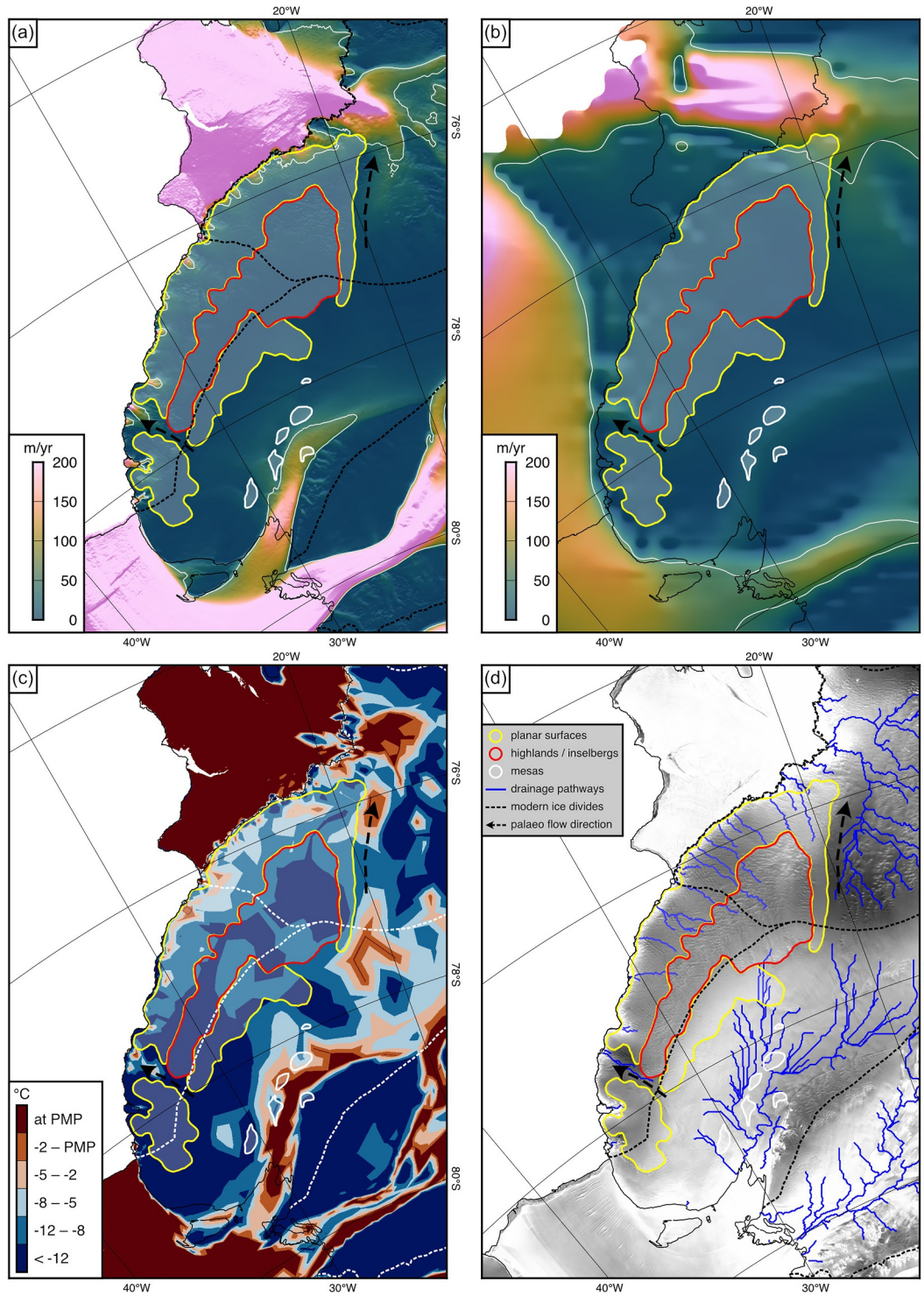

Figure 10. Present and past ice-sheet dynamics. (a) MEaSUREs observed present-day ice-surface velocity (Mouginot et al., 2019a). The white line demarcates the 50 m/yr contour. (b) Modeled Last Glacial Maximum ice-surface velocity snapshot at 20 ka (Albrecht et al., 2020). (c) Predicted basal temperatures derived from Ice-sheet and Sea-level System Model (ISSM) simulations of the present-day EAIS (Dawson et al., 2022). Temperatures are divided into six classes relative to the pressure melting point (PMP). (d) Predicted subglacial drainage pathways (blue lines) assuming basal meltwater follows the path of steepest hydropotential gradient (Livingstone et al., 2013).

incised. We note that these features may have originated as fluvial valleys that were subsequently overdeepened by ice or subglacial meltwater. We suggest that future targeted RES surveying in this region and quantification of valley morphology (e.g., dimensions, width-to-depth ratio, and cross-profile shape) would enable the relative roles of different styles of incision to be better distinguished (Van Der Vegt et al., 2012).

Differences in the degree of erosive modification by the ice sheet may also explain the comparative smoothness of PS3 compared to the rougher PS1/2 (Figure 3). If all three surfaces were similarly smooth prior to EAIS growth, the lower-lying coastal parts of PS1 would have subsequently been subjected to basal temperatures closer to the PMP (Figure 10c) and received more basal water flow (Figure 10d), causing minor scouring and incision of the topography (Hall & Sugden, 1987). By contrast, PS3 is higher, situated closer to the ice divide, and associated with lower basal temperatures, a negligible upstream drainage area, and minimal basal meltwater flow (Figures 10c and 10d); the persistence of these patterns throughout EAIS history would explain why this surface appears to be unmodified by glacial erosion.

The most conspicuous imprints of glacial erosion on the Coats Land landscape are the deep troughs bounding the planar surfaces. While these troughs likely originated as tectonic structures (Section 5.1), the overdeepening of their floors to ∼2 km below sea level (i.e., removal of post-rift sedimentary infill) implies that they have been selectively eroded by fast-flowing, warm-based ice. However, this is not occurring beneath the present-day EAIS; the ice within the Stancomb-Wills trough and the unnamed trough that separates PS3 from PS1/2 is largely stagnant and cold-based (Figures 10a and 10c). Therefore, we propose that EAIS configuration and behavior in Coats Land differed from today at some time in the past, with erosive ice flowing south-to-north either side of the Coats Land highlands (Figure 9c). This inference is supported by the presence of a topographic "gateway" connecting the upper reaches of the Recovery and Slessor Glaciers, which is interpreted as having been eroded via south-north palaeo-ice flow (Diez et al., 2018).

The most recent interval when the ice configuration differed from today was the Last Glacial Maximum (LGM; ca. 26–15 ka) (Peltier & Fairbanks, 2006), when the local EAIS surface was ∼300–650 m higher than today (Nichols et al., 2019) and the margin expanded to the continental shelf edge (Hillenbrand et al., 2014; Hodgson et al., 2018). However, the ice-flow direction implied by the sub-ice topography is difficult to reconcile with the orientation of bedforms from the last glacial cycle observed on the adjacent continental shelf, which are almost perpendicular to the onshore troughs (Arndt et al., 2020). Moreover, numerical modeling of the LGM ice sheet indicates that the flow pattern at this time was broadly comparable to today (Albrecht et al., 2020), with slow ice flow across Coats Land including over the unnamed trough east of PS3 and the Bailey trough (Figure 10b). These lines of evidence preclude the troughs being incised during the last glacial cycle and perhaps any period of similarly extensive ice cover during the Plio-Pleistocene.

Other candidate time intervals are the warm interglacial periods of the Pleistocene and/or Pliocene, when the EAIS may have experienced significant changes in configuration and extent (Cook et al., 2013; Crotti et al., 2022). Cosmogenic nuclide exposure ages extracted from rock samples in the Shackleton Range indicate limited, if any, ice cover since at least ca. 2.5 Ma, and potentially much longer (Fogwill et al., 2004; Sugden et al., 2014). Cosmogenic nuclide concentrations and geomorphological observations also imply that extremely low erosion rates have persisted over this time, indicative of regional climatic and ice-sheet stability. Pliocene ice-sheet modeling indicates that, while this interval may have witnessed ice-margin retreat within the Bailey, Slessor, and Recovery troughs (DeConto et al., 2021; Halberstadt et al., 2024), the EAIS did not reconfigure in such a way as to enable focussed northward flow through the now-stagnant troughs mapped in this study.

We therefore propose that the incision of the stagnant troughs in Coats Land most likely pre-dated the Pliocene. This is further supported by geomorphological evidence from the Shackleton Range, which indicates that pre-Pliocene regional ice-sheet behavior may have been substantially different from today. Striations, glacially smoothed bedrock, roches moutonnées, and glacial erratics of Beacon sandstone from the Whichaway Nunataks (Figure 1a) and limestones from the Pensacola Mountains (further south) indicate that, prior to the Pliocene (Sugden et al., 2014), the Shackleton Range was overridden by erosive, warm-based ice flowing from south to north (Höfle & Buggisch, 1995; Kerr & Hermichen, 1999). This flow direction is consistent with the orientation of the Stancomb-Wills trough, the unnamed trough east of PS3, and the Recovery-Slessor Gate (Diez et al., 2018) (Figure 9c). Cosmogenic nuclide exposure histories from the Ellsworth and Whitmore Mountains (west around the Weddell Sea Embayment) demonstrate that glacially eroded surfaces in this region also pre-date the Pliocene (Small et al., 2025; Spector et al., 2020; Sugden et al., 2017) and potentially formed prior to mid-Miocene (ca.

14 Ma) climate cooling and Antarctic Ice Sheet expansion (Shevenell et al., 2004). Overriding of the Pensacola Mountains by warm-based erosive ice is also constrained by cosmogenic nuclide exposure ages as having occurred significantly earlier than 3 Ma and most likely in the Miocene (Hodgson et al., 2012; Small et al., 2021).

EAIS expansion during one or more intervals of the Oligocene and/or early-to-mid-Miocene following initial ice-sheet growth at ca. 34 Ma but prior to the establishment of an arid polar climate at ca. 14 Ma (Shevenell et al., 2004; Spector & Balco, 2021) are therefore the most plausible periods for the incision of the south-to-north-oriented troughs in Coats Land. The locations of these outlets were likely governed by the inherited Jurassic rift structures (Figure 9c). An additional constraint on the age of these features is that they necessarily pre-date the incision of the deep Recovery and Slessor troughs. Otherwise, south-to-north ice flow would require ice to cross perpendicular to the Recovery trough, Shackleton Range, Slessor trough, and Theron Mountains (with variations in bed elevation of up to 4 km over horizontal scales of <50 km), which is glaciologically implausible. Indeed, the westward-flowing Recovery and Slessor catchments drain a large area of the EAIS (9.6 and 4.8 $\times$ 10^5 km^2, respectively) and once these systems had become established it is difficult to envisage how they could have been fundamentally reorganized. This is because the incision of the Slessor and Recovery troughs would have driven a positive feedback of selective trough excavation, isostatic uplift of the adjacent highlands, and differential basal thermal states within the troughs versus over the highlands (Sugden et al., 2014). This mechanism would have increasingly channeled fast-flowing (erosive) ice through the troughs and the catchments would have captured upstream ice from an increasingly wide area. A warm-based EAIS with a northward-sloping surface overriding the Shackleton Range would have only been feasible prior to the incision of the Recovery and Slessor troughs and concomitant uplift of the Shackleton Range and Theron Mountains, when the regional relief was greatly reduced (Paxman et al., 2019).

Since the exact timing of Recovery and Slessor incision is unconstrained, we simply suggest that, after a large-scale ice sheet first became established in East Antarctica, the existing rift-related structures in Coats Land were optimally oriented as conduits to steer northward ice flow (Figure 9c) (Kessler et al., 2008). We hypothesize that, at a later stage, westward flow through the Recovery and Slessor (and, to a lesser extent, Bailey) troughs became dominant, with the orientations of these features more favorably oriented for efficient drainage of a large upstream catchment. The resulting reorganization of ice flow would have reduced the drainage basin area (and erosive potential) of the ice within the Stancomb-Wills trough and the unnamed trough east of PS3, causing their stagnation and the subsequent preservation of the Coats Land landscape beneath slow-moving, cold-based ice (Figure 9d). We tentatively date the period characterized by south-to-north ice flow and trough incision in Coats Land to an early phase of continental-scale ice-sheet expansion in the Oligocene or early Miocene, prior to the widespread establishment of an arid polar climate in East Antarctica.

6. Conclusions

In this study, we have discovered and characterized extensive planar surfaces, rough highlands, and deep troughs within the subglacial landscape of Coats Land, East Antarctica. We draw four primary conclusions.

First, the subglacial troughs within Coats Land exhibit asymmetric cross-sectional profiles, steep escarpments, and mesa-like features commonly associated with Jurassic Ferrar dolerite intrusions in East Antarctica. We interpret these troughs to have originally formed during a period of crustal extension, most likely associated with Gondwana breakup in the Jurassic, which also triggered the flexural uplift of the adjacent highlands. Second, the planar surfaces on the coastward side of the highlands (when adjusted for the isostatic effects of ice loading and glacial erosion/sedimentation) are characterized by consistent elevations within 200 m of sea level and gentle offshore dips. Following the breakup of Gondwana, we suggest that erosion by fluvial systems over tens of millions of years resulted in the formation of a low-lying, gently inclined coastal plain. Third, the regional geomorphology indicates that during an early phase(s) of EAIS expansion (between 34 and 14 Ma), warm-based (erosive) ice flowed south-to-north across Coats Land, overriding the Shackleton Range and exploiting the inherited rift structures. This configuration was later abandoned as the Recovery and Slessor catchments were established by the mid-Miocene (Sugden et al., 2014). Fourth, the preservation of pre- and early-glacial landscapes in Coats Land is indicative of locally persistent non-erosive ice, characterized by low velocities and cold basal conditions. Fast ice flow is now dominated by the Recovery and Slessor Glaciers, whose underlying topography stabilizes the large-scale regional drainage patterns.

Conflict of Interest

The authors declare no conflicts of interest relevant to this study.

Data Availability Statement

The primary radio-echo sounding and aeromagnetic data used in this study are available at:

- BAS ICEGRAV (Ferraccioli et al., 2018, 2020)
- BAS FISS (Corr et al., 2024)
- NASA Operation IceBridge (Paden et al., 2010)
- AWI DML (Steinhage et al., 2023)

Other geospatial data sets used in this study are available at the following repositories:

- BedMachine Antarctica (Morlighem, 2022)
- MEaSUREs Antarctic ice velocity (Mouginot et al., 2019b)
- RADARSAT RAMP AMM-1 SAR mosaic (Jezek et al., 2013)
- ADMAP2B magnetic anomaly (Eagles et al., 2024)
- Isostatic response to ice sheet unloading (Paxman et al., 2022a)
- ISSM basal thermal state output (Dawson, 2022)
- Last glacial cycle model experiments (Albrecht, 2019)

Secondary data sets generated for this study are available via a Zenodo repository (Paxman, Jordan, et al., 2025).

Acknowledgments
Guy Paxman was supported by a Leverhulme Trust Early Career Fellowship (award number ECF-2021-549) and a Royal Society University Research Fellowship (award number URF\R1 \241308). Michael Bentley was supported by a Natural Environment Research Council Grant (NE/K003674/1) and by funding received from the European Research Council (ERC) under the European Union's Horizon 2020 research and innovation programme (grant agreement number 885205). David Small was supported by a Natural Environment Research Council Independent Research Fellowship (NE/T011963/1). The authors would like to thank the associate editor, Paul Winberry, along with three anonymous reviewers whose comments greatly improved the final manuscript. The authors would also like to extend thanks to C.D. Hillenbrand and Teal Riley for helpful discussions. This research is a contribution to the Scientific Committee on Antarctic Research Instabilities and Thresholds in Antarctica (INSTANT) programme and its Antarctic Geological Boundary Conditions (ABC) sub-committee. Figures were prepared using Generic Mapping Tools (Wessel et al., 2019) version 6 and colour palettes from Scientific Colour Maps (Crameri et al., 2020) version 7.

References

Aitken, A. R. A., Roberts, J. L., Ommen, T. D. V., Young, D. A., Golledge, N. R., Greenbaum, J. S., et al. (2016). Repeated large-scale retreat and advance of Totten Glacier indicated by inland bed erosion. *Nature*, *533*(7603), 385–389. https://doi.org/10.1038/nature17447

Albrecht, T. (2019). PISM glacial cycle sensitivity experiments of the Antarctic Ice Sheet (p. 1.8 GBytes) [Application/zip]. *PANGAEA*. https://doi.org/10.1594/PANGAEA.909727

Albrecht, T., Winkelmann, R., & Levermann, A. (2020). Glacial-cycle simulations of the Antarctic Ice Sheet with the Parallel Ice Sheet Model (PISM)—Part 1: Boundary conditions and climatic forcing. *The Cryosphere*, *14*(2), 599–632. https://doi.org/10.5194/tc-14-599-2020

Arndt, J. E., Larter, R. D., Hillenbrand, C.-D., Sørli, S. H., Forwick, M., Smith, J. A., & Wacker, L. (2020). Past ice sheet–seabed interactions in the northeastern Weddell Sea embayment, Antarctica. *The Cryosphere*, *14*(6), 2115–2135. https://doi.org/10.5194/tc-14-2115-2020

Bamber, J. L., Ferraccioli, F., Joughin, I., Shepherd, T., Rippin, D. M., Siegert, M. J., & Vaughan, D. G. (2006). East Antarctic ice stream tributary underlain by major sedimentary basin. *Geology*, *34*(1), 33. https://doi.org/10.1130/G22160.1

Barr, I. D., Spagnolo, M., Rea, B. R., Bingham, R. G., Oien, R. P., Adamson, K., et al. (2022). 60 million years of glaciation in the transantarctic mountains. *Nature Communications*, *13*(1), 5526. https://doi.org/10.1038/s41467-022-33310-z

Braun, J. (2018). A review of numerical modeling studies of passive margin escarpments leading to a new analytical expression for the rate of escarpment migration velocity. *Gondwana Research*, *53*, 209–224. https://doi.org/10.1016/j.gr.2017.04.012

Brook, D. (1972). Stratigraphy of the Theron Mountains. *British Antarctic Survey Bulletin*, *29*, 67–89.

Buck, W. R. (1991). Modes of continental lithospheric extension. *Journal of Geophysical Research*, *96*(B12), 20161–20178. https://doi.org/10.1029/91JB01485

Carter, C. M., Bentley, M. J., Jamieson, S. S. R., Paxman, G. J. G., Jordan, T. A., Bodart, J. A., et al. (2024). Extensive palaeo-surfaces beneath the Evans–Rutford region of the West Antarctic Ice Sheet control modern and past ice flow. *The Cryosphere*, *18*(5), 2277–2296. https://doi.org/10.5194/tc-18-2277-2024

Chang, M., Jamieson, S. S. R., Bentley, M. J., & Stokes, C. R. (2016). The surficial and subglacial geomorphology of western Dronning Maud Land, Antarctica. *Journal of Maps*, *12*(5), 892–903. https://doi.org/10.1080/17445647.2015.1097289

Chen, W., & Molnar, P. (1983). Focal depths of intracontinental and intraplate earthquakes and their implications for the thermal and mechanical properties of the lithosphere. *Journal of Geophysical Research*, *88*(B5), 4183–4214. https://doi.org/10.1029/JB088iB05p04183

Cockburn, H. A. P., Brown, R. W., Summerfield, M. A., & Seidl, M. A. (2000). Quantifying passive margin denudation and landscape development using a combined fission-track thermochronology and cosmogenic isotope analysis approach. *Earth and Planetary Science Letters*, *179*(3–4), 429–435. https://doi.org/10.1016/S0012-821X(00)00144-8

Contreras-Reyes, E., & Osses, A. (2010). Lithospheric flexure modelling seaward of the Chile trench: Implications for oceanic plate weakening in the trench outer rise region: Outer-rise flexure modelling off Chile. *Geophysical Journal International*, *182*(1), 97–112. https://doi.org/10.1111/j.1365-246X.2010.04629.x

Cook, C. P., Van De Flierdt, T., Williams, T., Hemming, S. R., Iwai, M., Kobayashi, M., et al. (2013). Dynamic behaviour of the East Antarctic ice sheet during Pliocene warmth. *Nature Geoscience*, *6*(9), 765–769. https://doi.org/10.1038/ngeo1889

Corr, H., Robinson, C., Jordan, T., Nicholls, K., Brisbourne, A., & Bodart, J. (2024). Processed airborne radio-echo sounding data from the FISS 2016 surveys covering the Filchner and Halley Ice Shelves, and the English Coast (western Palmer Land), West Antarctica (2016/2017)—V2 (Version 2.0, p. 115 files, 48.5 GB) [Dataset]. *NERC EDS UK Polar Data Centre*. https://doi.org/10.5285/E203926B-7A54-4C33-A5DF-04DF2293D7D3

Cox, S. C., Smith Lyttle, B., Elkind, S., Smith Siddoway, C. S., Morin, P., Capponi, G., et al. (2023). A continent-wide detailed geological map dataset of Antarctica. *Scientific Data*, *10*(1), 250. https://doi.org/10.1038/s41597-023-02152-9

Crameri, F., Shephard, G. E., & Heron, P. J. (2020). The misuse of colour in science communication. *Nature Communications*, *11*(1), 5444. https://doi.org/10.1038/s41467-020-19160-7

Crotti, I., Quiquet, A., Landais, A., Stenni, B., Wilson, D. J., Severi, M., et al. (2022). Wilkes subglacial basin ice sheet response to Southern Ocean warming during late Pleistocene interglacials. *Nature Communications*, *13*(1), 5328. https://doi.org/10.1038/s41467-022-32847-3

Dawson, E. J. (2022). ISSM results for Antarctic ice sheet basal thaw experiments [Dataset]. *Zenodo*. https://doi.org/10.5281/ZENODO.6870567

Dawson, E. J., Schroeder, D. M., Chu, W., Mantelli, E., & Seroussi, H. (2022). Ice mass loss sensitivity to the Antarctic ice sheet basal thermal state. *Nature Communications*, *13*(1), 4957. https://doi.org/10.1038/s41467-022-32632-2

DeConto, R. M., & Pollard, D. (2003). Rapid Cenozoic glaciation of Antarctica induced by declining atmospheric CO_2. *Nature*, *421*(6920), 245–249. https://doi.org/10.1038/nature01290

DeConto, R. M., Pollard, D., Alley, R. B., Velicogna, I., Gasson, E., Gomez, N., et al. (2021). The Paris climate agreement and future sea-level rise from Antarctica. *Nature*, *593*(7857), 83–89. https://doi.org/10.1038/s41586-021-03427-0

Diez, A., Matsuoka, K., Ferraccioli, F., Jordan, T. A., Corr, H. F., Kohler, J., et al. (2018). Basal settings control fast ice flow in the recovery/Slessor/bailey region, East Antarctica. *Geophysical Research Letters*, *45*(6), 2706–2715. https://doi.org/10.1002/2017GL076601

Eagles, G., Golynsky, A. V., Kim, H. R., Paxman, G. J. G., & Ferraccioli, F. (2024). ADMAP's Antarctic magnetic anomaly grids transformed for use with open source software (p. 18 data points) [Text/tab-separated-values]. *PANGAEA*. https://doi.org/10.1594/PANGAEA.965433

Elliot, D. H. (1992). Jurassic magmatism and tectonism associated with Gondwanaland break-up: An Antarctic perspective. *Geological Society, London, Special Publications*, *68*(1), 165–184. https://doi.org/10.1144/GSL.SP.1992.068.01.11

Ferraccioli, F., Corr, H., Jordan, T., Forsberg, R., Matsuoka, K., Diez, A., et al. (2018). Bed, surface elevation and ice thickness measurements derived from Radar acquired during the ICEGRAV-2013 airborne geophysics campaign (p. 845 MB) [Dataset]. *Polar Data Centre, Natural Environment Research Council*. https://doi.org/10.5285/6549203D-DA8B-4A22-924B-A9E1471EA7F1

Ferraccioli, F., Finn, C. A., Jordan, T. A., Bell, R. E., Anderson, L. M., & Damaske, D. (2011). East Antarctic rifting triggers uplift of the Gamburtsev Mountains. *Nature*, *479*(7373), 388–392. https://doi.org/10.1038/nature10566

Ferraccioli, F., Forsberg, R., Olesen, A., Jordan, T., Matsuoka, K., Zakrajsek, A., & Ghidella, M. (2020). Processed line aeromagnetic data over the Recovery Lakes region and interior Dronning Maud Land, East Antarctica (2013) (version 1.0, p. 1 file, 164 MB) [Dataset]. *UK Polar Data Centre, Natural Environment Research Council, UK Research & Innovation*. https://doi.org/10.5285/849E2215-95B0-4275-88B8-50E18E3F8D56

Ferraccioli, F., Jones, P. C., Curtis, M. L., & Leat, P. T. (2005). Subglacial imprints of early Gondwana break-up as identified from high resolution aerogeophysical data over western Dronning Maud Land, East Antarctica. *Terra Nova*, *17*(6), 573–579. https://doi.org/10.1111/j.1365-3121.2005.00651.x

Fogwill, C. J., Bentley, M. J., Sugden, D. E., Kerr, A. R., & Kubik, P. W. (2004). Cosmogenic nuclides ^{10}Be and ^{26}Al imply limited Antarctic Ice Sheet thickening and low erosion in the Shackleton Range for >1 m.y. *Geology*, *32*(3), 265. https://doi.org/10.1130/G19795.1

Forsberg, R., Olesen, A. V., Ferraccioli, F., Jordan, T. A., Matsuoka, K., Zakrajsek, A., et al. (2018). Exploring the recovery lakes region and interior Dronning Maud Land, East Antarctica, with airborne gravity, magnetic and radar measurements. *Geological Society, London, Special Publications*, *461*(1), 23–34. https://doi.org/10.1144/SP461.17

Franke, S., Eisermann, H., Jokat, W., Eagles, G., Asseng, J., Miller, H., et al. (2021). Preserved landscapes underneath the Antarctic Ice Sheet reveal the geomorphological history of Jutulstraumen Basin. *Earth Surface Processes and Landforms*, *46*(13), 2728–2745. https://doi.org/10.1002/esp.5203

Fretwell, P., Pritchard, H. D., Vaughan, D. G., Bamber, J. L., Barrand, N. E., Bell, R., et al. (2013). Bedmap2: Improved ice bed, surface and thickness datasets for Antarctica. *The Cryosphere*, *7*(1), 375–393. https://doi.org/10.5194/tc-7-375-2013

Garcia, E. S., Sandwell, D. T., & Luttrell, K. M. (2015). An iterative spectral solution method for thin elastic plate flexure with variable rigidity. *Geophysical Journal International*, *200*(2), 1012–1028. https://doi.org/10.1093/gji/ggu449

Golledge, N. R., Levy, R. H., McKay, R. M., & Naish, T. R. (2017). East Antarctic ice sheet most vulnerable to Weddell Sea warming. *Geophysical Research Letters*, *44*(5), 2343–2351. https://doi.org/10.1002/2016GL072422

Golynsky, A. V., Ferraccioli, F., Hong, J. K., Golynsky, D. A., Von Frese, R. R. B., Young, D. A., et al. (2018). New magnetic anomaly map of the Antarctic. *Geophysical Research Letters*, *45*(13), 6437–6449. https://doi.org/10.1029/2018GL078153

Halberstadt, A. R. W., Gasson, E., Pollard, D., Marschalek, J., & DeConto, R. M. (2024). Geologically constrained 2-million-year-long simulations of Antarctic Ice Sheet retreat and expansion through the Pliocene. *Nature Communications*, *15*(1), 7014. https://doi.org/10.1038/s41467-024-51205-z

Hall, A. M., & Sugden, D. E. (1987). Limited modification of mid-latitude landscapes by ice sheets: The case of northeast Scotland. *Earth Surface Processes and Landforms*, *12*(5), 531–542. https://doi.org/10.1002/esp.3290120510

Hillenbrand, C.-D., Bentley, M. J., Stolldorf, T. D., Hein, A. S., Kuhn, G., Graham, A. G. C., et al. (2014). Reconstruction of changes in the Weddell Sea sector of the Antarctic Ice Sheet since the Last Glacial Maximum. *Quaternary Science Reviews*, *100*, 111–136. https://doi.org/10.1016/j.quascirev.2013.07.020

Hochmuth, K., Gohl, K., Leitchenkov, G., Sauermilch, I., Whittaker, J. M., Uenzelmann-Neben, G., et al. (2020). The evolving paleobathymetry of the circum-Antarctic Southern Ocean since 34 ma: A key to understanding past cryosphere-ocean developments. *Geochemistry, Geophysics, Geosystems*, *21*(8), e2020GC009122. https://doi.org/10.1029/2020GC009122

Hodgson, D. A., Bentley, M. J., Schnabel, C., Cziferszky, A., Fretwell, P., Convey, P., & Xu, S. (2012). Glacial geomorphology and cosmogenic ^{10}Be and ^{26}Al exposure ages in the northern Dufek Massif, Weddell Sea embayment, Antarctica. *Antarctic Science*, *24*(4), 377–394. https://doi.org/10.1017/S0954102012000016

Hodgson, D. A., Hogan, K., Smith, J. M., Smith, J. A., Hillenbrand, C.-D., Graham, A. G. C., et al. (2018). Deglaciation and future stability of the Coats Land ice margin, Antarctica. *The Cryosphere*, *12*(7), 2383–2399. https://doi.org/10.5194/tc-12-2383-2018

Höfle, H. C., & Buggisch, W. (1995). Glacial geology and petrography of erratics in the Shackleton Range, Antarctica. *Polarforschung*, *63*(2–3), 183–201.

Jamieson, S. S. R., Ross, N., Paxman, G. J. G., Clubb, F. J., Young, D. A., Yan, S., et al. (2023). An ancient river landscape preserved beneath the East Antarctic Ice Sheet. *Nature Communications*, *14*(1), 6507. https://doi.org/10.1038/s41467-023-42152-2

Jamieson, S. S. R., Sugden, D. E., & Hulton, N. R. J. (2010). The evolution of the subglacial landscape of Antarctica. *Earth and Planetary Science Letters*, *293*(1–2), 1–27. https://doi.org/10.1016/j.epsl.2010.02.012

Jezek, K., Curlander, J., Carsey, F., Wales, C., & Barry, R. (2013). RAMP AMM-1 SAR image Mosaic of Antarctica, version 2 [Dataset]. *NASA National Snow and Ice Data Center Distributed Active Archive Center*. https://doi.org/10.5067/8AF4ZRPULS4H

Jordan, T. A., Ferraccioli, F., & Leat, P. T. (2017). New geophysical compilations link crustal block motion to Jurassic extension and strike-slip faulting in the Weddell Sea Rift System of West Antarctica. *Gondwana Research*, *42*, 29–48. https://doi.org/10.1016/j.gr.2016.09.009

Jordan, T. A., Ferraccioli, F., Ross, N., Corr, H. F. J., Leat, P. T., Bingham, R. G., et al. (2013). Inland extent of the Weddell Sea Rift imaged by new aerogeophysical data. *Tectonophysics*, *585*, 137–160. https://doi.org/10.1016/j.tecto.2012.09.010

Kerr, A. R., & Hermichen, W. D. (1999). Glacial modification of the Shackleton Range, Antarctica. *Terra Antarctica*, *6*(3), 353–360.

Kessler, M. A., Anderson, R. S., & Briner, J. P. (2008). Fjord insertion into continental margins driven by topographic steering of ice. *Nature Geoscience*, *1*(6), 365–369. https://doi.org/10.1038/ngeo201

Kleinschmidt, G., & Boger, S. (2009). The Bertrab, Littlewood and Moltke Nunataks of Prinz-Regent-Luitpold-Land (Coats Land)—Enigma of East Antarctic Geology. *Polarforschung*, *78*(3), 95–104.

Krohne, N., Lisker, F., Kleinschmidt, G., Klügel, A., Läufer, A., Estrada, S., & Spiegel, C. (2018). The Shackleton Range (East Antarctica): An alien block at the rim of Gondwana? *Geological Magazine*, *155*(4), 841–864. https://doi.org/10.1017/S0016756816001011

Lai, C.-Y., Kingslake, J., Wearing, M. G., Chen, P.-H. C., Gentine, P., Li, H., et al. (2020). Vulnerability of Antarctica's ice shelves to meltwater-driven fracture. *Nature*, *584*(7822), 574–578. https://doi.org/10.1038/s41586-020-2627-8

Lavier, L. L., & Buck, W. R. (2002). Half graben versus large-offset low-angle normal fault: Importance of keeping cool during normal faulting. *Journal of Geophysical Research*, *107*(B6). https://doi.org/10.1029/2001JB000513

Le Brocq, A. M., Hubbard, A., Bentley, M. J., & Bamber, J. L. (2008). Subglacial topography inferred from ice surface terrain analysis reveals a large un-surveyed basin below sea level in East Antarctica. *Geophysical Research Letters*, *35*(16), 2008GL034728. https://doi.org/10.1029/2008GL034728

Livingstone, S. J., Clark, C. D., Woodward, J., & Kingslake, J. (2013). Potential subglacial lake locations and meltwater drainage pathways beneath the Antarctic and Greenland ice sheets. *The Cryosphere*, *7*(6), 1721–1740. https://doi.org/10.5194/tc-7-1721-2013

MacGregor, J. A., Boisvert, L. N., Medley, B., Petty, A. A., Harbeck, J. P., Bell, R. E., et al. (2021). The Scientific Legacy of NASA's Operation IceBridge. *Reviews of Geophysics*, *59*(2), e2020RG000712. https://doi.org/10.1029/2020RG000712

Maritati, A., Danišík, M., Halpin, J. A., Whittaker, J. M., & Aitken, A. R. A. (2020). Pangea rifting shaped the East Antarctic landscape. *Tectonics*, *39*(8), e2020TC006180. https://doi.org/10.1029/2020TC006180

Marsh, P. D. (1985). Ice surface and bedrock topography in Coats Land and part of Dronning Maud Land, Antarctica, from Satellite Imagery. *British Antarctic Survey Bulletin*, *68*, 19–36.

Mieth, M., & Jokat, W. (2014). New aeromagnetic view of the geological fabric of southern Dronning Maud Land and Coats Land, East Antarctica. *Gondwana Research*, *25*(1), 358–367. https://doi.org/10.1016/j.gr.2013.04.003

Miller, K. G., Schmelz, W. J., Browning, J. V., Rosenthal, Y., Hess, A. V., Kopp, R. E., & Wright, J. D. (2024). Global mean and relative sea-level changes over the past 66 Myr: Implications for early Eocene ice sheets. *Earth Science, Systems and Society*, *3*(1), 10091. https://doi.org/10.3389/esss.2023.10091

Morlighem, M. (2022). MEaSUREs BedMachine Antarctica, version 3 [Dataset]. *NASA National Snow and Ice Data Center Distributed Active Archive Center*. https://doi.org/10.5067/FPSU0V1MWUB6

Morlighem, M., Rignot, E., Binder, T., Blankenship, D., Drews, R., Eagles, G., et al. (2020). Deep glacial troughs and stabilizing ridges unveiled beneath the margins of the Antarctic ice sheet. *Nature Geoscience*, *13*(2), 132–137. https://doi.org/10.1038/s41561-019-0510-8

Mouginot, J., Rignot, E., & Scheuchl, B. (2019a). Continent-wide, interferometric SAR phase, mapping of Antarctic ice velocity. *Geophysical Research Letters*, *46*(16), 9710–9718. https://doi.org/10.1029/2019GL083826

Mouginot, J., Rignot, E., & Scheuchl, B. (2019b). MEaSUREs phase-based Antarctica ice velocity map, version 1 [Dataset]. *NASA National Snow and Ice Data Center Distributed Active Archive Center*. https://doi.org/10.5067/PZ3NJ5RXRH10

Müller, R. D., Seton, M., Zahirovic, S., Williams, S. E., Matthews, K. J., Wright, N. M., et al. (2016). Ocean basin evolution and global-scale plate reorganization events since Pangea breakup. *Annual Review of Earth and Planetary Sciences*, *44*(1), 107–138. https://doi.org/10.1146/annurev-earth-060115-012211

Nichols, K. A., Goehring, B. M., Balco, G., Johnson, J. S., Hein, A. S., & Todd, C. (2019). New Last Glacial Maximum ice thickness constraints for the Weddell Sea Embayment, Antarctica. *The Cryosphere*, *13*(11), 2935–2951. https://doi.org/10.5194/tc-13-2935-2019

Nixdorf, U., Steinhage, D., Meyer, U., Hempel, L., Jenett, M., Wachs, P., & Miller, H. (1999). The newly developed airborne radio-echo sounding system of the AWI as a glaciological tool. *Annals of Glaciology*, *29*, 231–238. https://doi.org/10.3189/172756499781821346

Otosaka, I. N., Shepherd, A., Ivins, E. R., Schlegel, N.-J., Amory, C., Van Den Broeke, M. R., et al. (2023). Mass balance of the Greenland and Antarctic ice sheets from 1992 to 2020. *Earth System Science Data*, *15*(4), 1597–1616. https://doi.org/10.5194/essd-15-1597-2023

Paden, J., Li, J., Leuschen, C., Rodriguez-Morales, F., & Hale, R. (2010). IceBridge MCoRDS L2 ice thickness, version 1 [Dataset]. *NASA National Snow and Ice Data Center Distributed Active Archive Center*. https://doi.org/10.5067/GDQ0CUCVTE2Q

Pattyn, F., & Morlighem, M. (2020). The uncertain future of the Antarctic Ice Sheet. *Science*, *367*(6484), 1331–1335. https://doi.org/10.1126/science.aaz5487

Paxman, G. J. G. (2023). Antarctic palaeotopography. *Geological Society*, *56*(1), 231–251. https://doi.org/10.1144/M56-2020-7

Paxman, G. J. G., Austermann, J., & Hollyday, A. (2022a). Grid files of the total isostatic response to the complete unloading of the Greenland and Antarctic Ice Sheets (version 2) [Dataset]. *NSF Arctic Data Center*. https://doi.org/10.18739/A2WS8HN3C

Paxman, G. J. G., Austermann, J., & Hollyday, A. (2022b). Total isostatic response to the complete unloading of the Greenland and Antarctic Ice Sheets. *Scientific Reports*, *12*(1), 11399. https://doi.org/10.1038/s41598-022-15440-y

Paxman, G. J. G., Jamieson, S. S. R., Ferraccioli, F., Bentley, M. J., Forsberg, R., Ross, N., et al. (2017). Uplift and tilting of the Shackleton Range in East Antarctica driven by glacial erosion and normal faulting. *Journal of Geophysical Research: Solid Earth*, *122*(3), 2390–2408. https://doi.org/10.1002/2016JB013841

Paxman, G. J. G., Jamieson, S. S. R., Hochmuth, K., Gohl, K., Bentley, M. J., Leitchenkov, G., & Ferraccioli, F. (2019). Reconstructions of Antarctic topography since the Eocene–Oligocene boundary. *Palaeogeography, Palaeoclimatology, Palaeoecology*, *535*, 109346. https://doi.org/10.1016/j.palaeo.2019.109346

Paxman, G. J. G., Jamieson, S. S. R., Ross, N., Bentley, M. J., Carter, C. M., Jordan, T. A., et al. (2025). Extensive fluvial surfaces at the East Antarctic margin have modulated ice-sheet evolution. *Nature Geoscience*, *18*(8), 724–731. https://doi.org/10.1038/s41561-025-01734-z

Paxman, G. J. G., Jordan, T. A., Bentley, M. J., Small, D., Jamieson, S. S. R., & Steinhage, D. (2025). Subglacial topography of Coats Land records post-Gondwanan landscape evolution and early ice-sheet behaviour in East Antarctica: Datasets (version 1.0) [Dataset]. *Zenodo*. https://doi.org/10.5281/ZENODO.17224909

Peltier, W. R., & Fairbanks, R. G. (2006). Global glacial ice volume and Last Glacial Maximum duration from an extended Barbados sea level record. *Quaternary Science Reviews*, *25*(23–24), 3322–3337. https://doi.org/10.1016/j.quascirev.2006.04.010

Pritchard, H. D., Fretwell, P. T., Fremand, A. C., Bodart, J. A., Kirkham, J. D., Aitken, A., et al. (2025). Bedmap3 updated ice bed, surface and thickness gridded datasets for Antarctica. *Scientific Data*, *12*(1), 414. https://doi.org/10.1038/s41597-025-04672-y

Rignot, E., Bamber, J. L., Van Den Broeke, M. R., Davis, C., Li, Y., Van De Berg, W. J., & Van Meijgaard, E. (2008). Recent Antarctic ice mass loss from radar interferometry and regional climate modelling. *Nature Geoscience*, *1*(2), 106–110. https://doi.org/10.1038/ngeo102

Riley, T. R., Jordan, T. A., Leat, P. T., Curtis, M. L., & Millar, I. L. (2020). Magmatism of the Weddell Sea rift system in Antarctica: Implications for the age and mechanism of rifting and early stage Gondwana breakup. *Gondwana Research*, *79*, 185–196. https://doi.org/10.1016/j.gr.2019.09.014

Rippin, D. M., Siegert, M. J., Bamber, J. L., Vaughan, D. G., & Corr, H. F. J. (2006). Switch-off of a major enhanced ice flow unit in East Antarctica. *Geophysical Research Letters*, *33*(15), 2006GL026648. https://doi.org/10.1029/2006GL026648

Rose, K. C., Ferraccioli, F., Jamieson, S. S. R., Bell, R. E., Corr, H., Creyts, T. T., et al. (2013). Early East Antarctic Ice Sheet growth recorded in the landscape of the Gamburtsev Subglacial Mountains. *Earth and Planetary Science Letters*, *375*, 1–12. https://doi.org/10.1016/j.epsl.2013.03.053

Rose, K. C., Ross, N., Jordan, T. A., Bingham, R. G., Corr, H. F. J., Ferraccioli, F., et al. (2015). Ancient pre-glacial erosion surfaces preserved beneath the West Antarctic Ice Sheet. *Earth Surface Dynamics*, *3*(1), 139–152. https://doi.org/10.5194/esurf-3-139-2015

Ross, N., Jordan, T. A., Bingham, R. G., Corr, H. F. J., Ferraccioli, F., Le Brocq, A., et al. (2014). The Ellsworth subglacial highlands: Inception and retreat of the West Antarctic ice sheet. *Geological Society of America Bulletin*, *126*(1–2), 3–15. https://doi.org/10.1130/B30794.1

Seroussi, H., Nowicki, S., Payne, A. J., Goelzer, H., Lipscomb, W. H., Abe-Ouchi, A., et al. (2020). ISMIP6 Antarctica: A multi-model ensemble of the Antarctic ice sheet evolution over the 21st century. *The Cryosphere*, *14*(9), 3033–3070. https://doi.org/10.5194/tc-14-3033-2020

Shepard, M. K., Campbell, B. A., Bulmer, M. H., Farr, T. G., Gaddis, L. R., & Plaut, J. J. (2001). The roughness of natural terrain: A planetary and remote sensing perspective. *Journal of Geophysical Research*, *106*(E12), 32777–32795. https://doi.org/10.1029/2000JE001429

Shevenell, A. E., Kennett, J. P., & Lea, D. W. (2004). Middle Miocene Southern Ocean cooling and Antarctic cryosphere expansion. *Science*, *305*(5691), 1766–1770. https://doi.org/10.1126/science.1100061

Small, D., Bentley, M. J., Evans, D. J. A., Hein, A. S., & Freeman, S. P. H. T. (2021). Ice-free valleys in the Neptune Range of the Pensacola Mountains, Antarctica: Glacial geomorphology, geochronology and potential as palaeoenvironmental archives. *Antarctic Science*, *33*(4), 428–455. https://doi.org/10.1017/S0954102021000237

Small, D., Bentley, M. J., Freeman, S. P. H. T., Rodés, A., & Xu, S. (2025). A pre-Pliocene origin of the glacial trimline in the Ellsworth Mountains and the prevalence of old landscapes at high elevations in West Antarctica. *Geomorphology*, *473*, 109634. https://doi.org/10.1016/j.geomorph.2025.109634

Spector, P., & Balco, G. (2021). Exposure-age data from across Antarctica reveal mid-Miocene establishment of polar desert climate. *Geology*, *49*(1), 91–95. https://doi.org/10.1130/G47783.1

Spector, P., Stone, J., Balco, G., Hillebrand, T., Thompson, M., & Black, T. (2020). Miocene to Pleistocene glacial history of West Antarctica inferred from Nunatak geomorphology and cosmogenic-nuclide measurements on bedrock surfaces. *American Journal of Science*, *320*(8), 637–676. https://doi.org/10.2475/10.2020.01

Steinhage, D., Franke, S., Eisen, O., Miller, H., & Helm, V. (2023). Ice thickness from western and central Dronning Maud Land (Antarctica) recorded with the airborne AWI EMR radar system in 2002/2003 (p. 100005 data points) [Text/tab-separated-values]. *PANGAEA*. https://doi.org/10.1594/PANGAEA.957062

Stokes, C. R., Abram, N. J., Bentley, M. J., Edwards, T. L., England, M. H., Foppert, A., et al. (2022). Response of the East Antarctic Ice Sheet to past and future climate change. *Nature*, *608*(7922), 275–286. https://doi.org/10.1038/s41586-022-04946-0

Studinger, M., Bell, R. E., Buck, W. R., Karner, G. D., & Blankenship, D. D. (2004). Sub-ice geology inland of the Transantarctic Mountains in light of new aerogeophysical data. *Earth and Planetary Science Letters*, *220*(3–4), 391–408. https://doi.org/10.1016/S0012-821X(04)00066-4

Studinger, M., & Miller, H. (1999). Crustal structure of the Filchner-Ronne Shelf and Coats Land, Antarctica, from gravity and magnetic data: Implications for the breakup of Gondwana. *Journal of Geophysical Research*, *104*(B9), 20379–20394. https://doi.org/10.1029/1999JB900117

Sugden, D. E., Fogwill, C. J., Hein, A. S., Stuart, F. M., Kerr, A. R., & Kubik, P. W. (2014). Emergence of the Shackleton Range from beneath the Antarctic Ice Sheet due to glacial erosion. *Geomorphology*, *208*, 190–199. https://doi.org/10.1016/j.geomorph.2013.12.004

Sugden, D. E., Hein, A. S., Woodward, J., Marrero, S. M., Rodés, Á., Dunning, S. A., et al. (2017). The million-year evolution of the glacial trimline in the southernmost Ellsworth Mountains, Antarctica. *Earth and Planetary Science Letters*, *469*, 42–52. https://doi.org/10.1016/j.epsl.2017.04.006

Sugden, D. E., & Jamieson, S. S. R. (2018). The pre-glacial landscape of Antarctica. *Scottish Geographical Journal*, *134*(3–4), 203–223. https://doi.org/10.1080/14702541.2018.1535090

Sugden, D. E., Marchant, D. R., Potter, N., Souchez, R. A., Denton, G. H., Swisher, C. C., III., & Tison, J.-L. (1995). Preservation of Miocene glacier ice in East Antarctica. *Nature*, *376*(6539), 412–414. https://doi.org/10.1038/376412a0

Swain, C. J., & Kirby, J. F. (2021). Effective Elastic thickness map reveals subglacial structure of East Antarctica. *Geophysical Research Letters*, *48*(4), e2020GL091576. https://doi.org/10.1029/2020GL091576

Tessensohn, F., Kleinschmidt, G., Talarico, F., Buggisch, W., Brommer, A., Henjes-Kunst, F., et al. (1999). Ross-age amalgamation of East and West Gondwana: Evidence from the Shackleton range. *Terra Antarctica*, *6*(3), 317–325.

Van Der Vegt, P., Janszen, A., & Moscariello, A. (2012). Tunnel valleys: Current knowledge and future perspectives. *Geological Society*, *368*(1), 75–97. https://doi.org/10.1144/SP368.13

Vaughan, D. G., Barnes, D. K. A., Fretwell, P. T., & Bingham, R. G. (2011). Potential seaways across West Antarctica. *Geochemistry, Geophysics, Geosystems*, *12*(10). https://doi.org/10.1029/2011GC003688

Watts, A. B. (2001). *Isostasy and flexure of the lithosphere*. Cambridge University Press.

Weissel, J. K., & Karner, G. D. (1989). Flexural uplift of rift flanks due to mechanical unloading of the lithosphere during extension. *Journal of Geophysical Research*, *94*(B10), 13919–13950. https://doi.org/10.1029/JB094iB10p13919

Wessel, P., Luis, J. F., Uieda, L., Scharroo, R., Wobbe, F., Smith, W. H. F., & Tian, D. (2019). The generic mapping tools version 6. *Geochemistry, Geophysics, Geosystems*, *20*(11), 5556–5564. https://doi.org/10.1029/2019GC008515

Whitehouse, P. L., Gomez, N., King, M. A., & Wiens, D. A. (2019). Solid Earth change and the evolution of the Antarctic Ice Sheet. *Nature Communications*, *10*(1), 503. https://doi.org/10.1038/s41467-018-08068-y

Will, T. M., Zeh, A., Gerdes, A., Frimmel, H. E., Millar, I. L., & Schmädicke, E. (2009). Palaeoproterozoic to Palaeozoic magmatic and metamorphic events in the Shackleton Range, East Antarctica: Constraints from zircon and monazite dating, and implications for the amalgamation of Gondwana. *Precambrian Research*, *172*(1–2), 25–45. https://doi.org/10.1016/j.precamres.2009.03.008